Applied Energy 368 (2024) 123355

Contents lists available at ScienceDirect

Applied Energy

journal homepage: www.elsevier.com/locate/apenergy

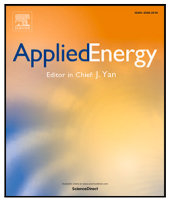

Microgrid design and multi-year dispatch optimization under climate-informed load and renewable resource uncertainty

Madeline Macmillan [a,b], Alexander Zolan [b,*], Morgan Bazilian [c], Daniel L. Villa [d]

[a] Colorado School of Mines, Advanced Energy Systems Program, 1500 Illinois Street, Golden, CO 80401, United States of America
[b] National Renewable Energy Laboratory, 15013 Denver West Parkway, Golden, CO 80401, United States of America
[c] Colorado School of Mines, Payne Institute, 1500 Illinois Street, Golden, CO 80401, United States of America
[d] Sandia National Laboratories, 1515 Eubank Blvd., Albuquerque, NM 87123-0710, United States of America

ARTICLE INFO

Keywords:
Energy systems
Microgrids
Stochastic programming
Climate change
Resilience

ABSTRACT

Microgrids are an increasingly popular solution to provide energy resilience in response to increasing grid dependency and the growing impacts of climate change on grid operations. However, existing microgrid models do not currently consider the uncertain and long-term impacts of climate change when determining a set of design and operational decisions to minimize long-term costs or meet a resilience threshold. In this paper, we develop a novel scenario generation method that accounts for the uncertain effects of (i) climate change on variable renewable energy availability, (ii) extreme heat events on site load, and (iii) population and electrification trends on load growth. Additionally, we develop a two-stage stochastic programming extension of an existing microgrid design and dispatch optimization model to obtain uncertainty-informed and climate-resilient energy system decisions that minimizes long-term costs. Use of sample average approximation to validate our two case studies illustrates that the proposed methodology produces high-quality solutions that add resilience to systems with existing backup generation while reducing expected long-term costs.

1. Introduction

1.1. Background and motivation

Society is dependent on energy systems and the services they support such as security, healthcare, transportation, and communication. Resilience of energy systems is gaining interest due to the grid's increasing vulnerability to disruptions from severe weather events [1,2]. Losses due to climate change-driven extreme heat have been estimated as between $5 trillion and $29.3 trillion globally with more than 80% of the economic losses absorbed by disadvantaged populations [3]. Extreme heat also increases electric loads significantly [4] and limits the capacity of power plants [5], increasing the frequency of outages.

In recent history, climate-driven extreme temperature events have caused outages costing the United States economy billions of dollars in lost productivity and physical damages [6]. These events can lead to hazardous conditions for large populations due to heat exposure in buildings [7]. The observed trends of increasing frequency and severity of these expensive events [8] motivate our approach of optimizing microgrid designs and measuring their resilience in longer-term operating periods.

The outputs from microgrid design tools and planning models typically include deployment of Distributed Energy Resources (DER), and load management recommendations [9]. DERs are energy-generating and storage technologies that are directly connected to small distribution systems which, in turn, may or may not be connected to the bulk power system [10]. Microgrids are networks of DERs that can operate without connection to the grid [11]. Microgrids that include renewable DERs can provide reductions in utility expenditures and, when paired with storage, may add resilience to the networked loads within the microgrid [12]. Non-renewable DERs, such as diesel generators, can be included in a microgrid design to provide power when it is economical to do so, or when renewable and storage technologies are not sufficient to meet demand during a grid outage. However, diesel generators require a non-renewable fuel source, and fuel prices incentivize the use of co-located renewables and/or storage to manage costs, especially in remote locations [13]. Rules of thumb are typically not cost effective in microgrid planning decisions, so tools have been developed which employ optimization techniques to inform DER sizing and operations for residential and commercial customers [14].

* Corresponding author.
E-mail addresses: madelinemacmillan@mines.edu (M. Macmillan), alexander.zolan@nrel.gov (A. Zolan), mbazilian@mines.edu (M. Bazilian), dlvilla@sandia.gov (D.L. Villa).

https://doi.org/10.1016/j.apenergy.2024.123355
Received 27 October 2023; Received in revised form 30 March 2024; Accepted 30 April 2024
Available online 28 May 2024

Acronyms

AUC	Area Under the Curve
BAU	Business As Usual
CI	Confidence Interval
CMIP6	6th Coupled Model Intercomparison Project
DER	Distributed Energy Resources
EV	Expected Value
EVSS	Expected Value of the Stochastic Solution
HW	Heat Wave
IPCC	Intergovernmental Panel on Climate Change
LCC	Life-Cycle Cost
MDT	Microgrid Design Toolkit
MEWS	Multi-scenario Extreme Weather Simulator
NOAA	National Oceanic and Atmospheric Administration
OOS	Out-of-Sample
PV	Photovoltaic
RCP	Representative Concentration Pathways
RP	Recourse Problem
SAA	Sample Average Approximation
SSP	Shared Socio-economic Pathways
TMY	Typical Meteorological Year
VoLL	Value of Lost Load
VRE	Variable Renewable Energy

In light of climate change and the associated severe weather events posing threats to energy systems, recent studies have incorporated resilience considerations into planning decisions for both microgrids and broader energy systems. Perera et al. [15] develop a modeling framework that optimizes microgrid designs for communities vulnerable to wildfires. However, this study does not consider uncertainties associated with climate change and the subsequent impact they may have on the energy demand, energy supply, and resilience of the system. Totschnig et al. [16] use an hourly simulation model to assess the impact of climate change on the resilience of the electricity sector for Austria and Germany. For campus-sized and remote, grid-disconnected microgrids that may grow with the broader population, load growth due to population growth and electrification should be considered [17].

The first contribution of this paper is a methodology that generates multi-year scenarios for microgrid optimization models that incorporate uncertainty in: (i) climate-related impacts to energy demand; (ii) long-term population growth and electrification of buildings; and, (iii) uncertainty in Variable Renewable Energy (VRE) resources. Our simulation assumes that these three factors are stochastic in nature and independent of each other. Our second contribution extends an existing microgrid design and dispatch optimization model, REopt [18], to obtain solutions under uncertainty by recasting the single-year, deterministic REopt model as a two-stage stochastic program in which each scenario includes multiple years of operational decisions. The DERs available to meet electrical loads in REopt include diesel generators, photovoltaics (PV), wind turbines, batteries, and combined heat and power systems; thermal generation and storage technologies are also available to model the service of thermal loads on site. Our extension of the existing work allows a user to obtain microgrid design decisions that account for multiple, multi-year scenarios of VRE and load, rather than a deterministic model with a single year of operations. We hypothesize that our novel methodology will obtain microgrid design and dispatch decisions lower expected long-term costs when compared to other scenario generation methods that incorporate fewer sources of uncertainty. We use sample average approximation [19] to obtain estimates of long-term costs and test this hypothesis.

1.2. Literature review

Within this study, we consider a microgrid design and dispatch model that can measure resilience while considering the uncertain effects of population growth and electrification, climate change, and VRE generation. Below, we subdivide the relevant literature into sections on software tools, stochastic models, optimization under uncertainty, and long-term planning models.

1.2.1. Microgrid planning software tools

Many models exist for microgrid planning and resilience, and they differ by structure, technologies considered, and objective. Reviews from Ringkjøb et al. [9] and Wang et al. [20] provide an overview of energy system and microgrid planning tools, including commonly used software such as REopt [21], HOMER [22], Microgrid Design Toolkit (MDT) [23], and DER-CAM [24]. These models obtain microgrid designs and operational decisions using either a search algorithm or a mixed-integer linear program, and can conduct sensitivity analyses. REopt, MDT, and DER-CAM consider neither multi-year nor multi-scenario customizations [25] while a multi-year module of HOMER can consider load and capital expense changes [26,27]. The methodology in this paper augments REopt's existing capabilities by developing a scenario generation method and a two-stage stochastic programming formulation.

1.2.2. Microgrid uncertainty models

Incorporating uncertainty is an increasingly important component of microgrid and resilience assessments, as shown by Robert and Gopalan's work demonstrating that a dependence on an individual solar generation forecast results in unanticipated shortages [28]. Monte Carlo simulations, Markov reward processes, and sensitivity analyses have been used to incorporate uncertainty within energy system planning models and resilience assessments. Panteli and Mancarella [29] develop a Monte Carlo simulation to compare normal, robust, redundant, and responsive resilience strategies in a high-wind environment. Younesi et al. [30] use Monte Carlo simulations with a three-state chain Markov reward processes to evaluate the resilience of interconnected energy system components. Two common limiting factors with Monte Carlo simulations and Markov reward processes are available data with which to populate the probability distributions within the model and solution time. Sensitivity analyses demonstrate the impacts of input changes on decisions, as implemented in Totschnig et al. and Ascione et al. to assess and design resilient energy systems, respectively [16,31]. While sensitivity analysis is less data-intensive than Markov reward processes, each instance assumes certainty in the inputs. In response to these restrictions and the available data for our approach, we apply stochastic programming and sample multiple time-series VRE profiles to mitigate overfitting a system design to a single forecast while providing upper and lower bounds on the expected long-term cost of the optimal solution.

1.2.3. Microgrid optimization under uncertainty

Microgrid planning models that incorporate uncertainty in both load and VRE resources commonly focus on dispatch operations. Wang et al. [32] develop a multi-objective approach to dispatch multiple microgrids under load and renewable resource uncertainty in which they minimize costs and emissions generation; their approach is intended to be robust to sudden drops in intermittent VRE availability, and they use a heuristic to obtain dispatch decisions. Konneh et al. [33] summarize works that employ model predictive control to adapt to sudden changes in load, and recent work by Hans et al. [34] extends this method to cover islanded grid operations in a risk-averse framework. Xiang et al. [35] present a robust optimization model to obtain cost-minimizing and social benefit-maximizing dispatch decisions, in which they incorporate uncertainty in both renewable generation and

load using historical data from which they obtain point and interval estimates; the authors utilize an orthogonal array to determine the uncertainty set for their solution method, and then use Monte Carlo sampling to verify solution quality. Wang et al. [36] present a two-stage stochastic program that obtains expected cost-minimizing dispatch decisions for multiple microgrids which interact with a central utility; the utility decisions take place in the first stage while the second stage determines the dispatch of the individual microgrids, and they utilize a sequential sampling approach to generate scenarios of load and renewables generation. Similar to the work in [35,36], we use mathematical programming to obtain planning decisions, but we include the capacities of generating technologies and storage systems as design considerations.

Stochastic programming formulations that consider both design and dispatch decisions for microgrids address the computational burden of the planning problem by use of a combination of approximations, heuristics, and truncated time horizons. Han and Lee [37] develop a planning model for a multi-microgrid system in which the first stage considers connections between renewable-powered microgrids, the second stage considers individual microgrid operations over 24-h dispatch periods, and the objective is to minimize capital and expected operational costs. Like the work of Han and Lee, we consider a two-stage approach, but our first stage considers the sizing of the generators under the assumption that the microgrid shares a single bus, while Han and Lee consider connections between generators and loads in the first stage and assume fixed generator sizing.

1.2.4. Long-term planning models

The long life of assets purchased for energy system planning decisions motivates us to investigate load growth due to population and electrification trends. Takalani and Bekker's rural microgrid assessment highlights the significance of "future proofing" when making long-term energy system plans [17]. Similar to Takalani and Bekker, we adopt long-term population growth considerations to generate scenarios that are informed and connected by multi-year load growth assumptions. A key distinction that was not identified in the literature was the application of these considerations in cases beyond rural locations such as the (grid-connected) case studies we explore. While grid-connected microgrids do not suffer outages during normal operations, accounting for future growth can change the most economical design, as well as resilience metrics in out-years when compared to the solutions obtained from a single-year, deterministic model. This motivates the development of our methodology to generate multi-year scenarios as we describe in Section 2.

The rest of this paper is organized as follows. Section 2 describes models, assumptions, and formulations used in this study. Section 3 presents the results from the analysis. Section 4 summarizes the key takeaways of this assessment and proposes next steps.

2. Methodology

This section details the methodology that we employ to generate independent and identically distributed scenarios that span multiple years and serve as input to a microgrid design and dispatch optimization model. The scenarios we generate incorporate uncertainty in (i) the impacts of climate change on load, (ii) the impacts of climate change on VRE availability, and (iii) load growth in out-years of microgrid operations. Fig. 1 displays the inputs and outputs of each model that we employ in our framework, as well as interactions between models.

To consider the anticipated impacts of climate change on extreme temperature events which, in turn, affect load profiles, we use the Multi-scenario Extreme Weather Simulator (MEWS). MEWS uses National Oceanic and Atmospheric Administration (NOAA) daily summaries and US climate normals [38] data to fit a stochastic model to historic heat wave and cold snap patterns. MEWS then shifts these patterns using the 6th Coupled Model Intercomparison Project (CMIP6) surface temperature for a chosen future year and Shared Socio-economic Pathways (SSP) and Intergovernmental Panel on Climate Change (IPCC) shifts in the frequency and intensity of Heat Wave (HW) events. The resulting HW distributions for future conditions are used to develop climate-informed, hourly load profiles with EnergyPlus which we then further adjust for projected growth due to electrification and population growth in future years. We simulate VRE profiles by randomly selecting (i) historical year-long profiles at hourly fidelity, and (ii) growth factors from probability distributions informed by projections in the literature.

The load profiles are then combined with VRE profiles, the electricity tariff, and technological specifications as inputs to our optimization model, which solves multiple single-year instances of REopt. Our methodology outputs a recommended design as well as its expected lifecycle cost and resilience measures. The specific electrical and thermal technologies that may be procured and operate to meet site loads within REopt are summarized in Fig. 2, and the case study descriptions in Section 3.1 specify which subset of technologies is available in each instance.

2.1. Extreme weather and developing climate-adjusted loads

The Representative Concentration Pathways (RCP) and SSP from the IPCC [2,39] are commonly used methods to generate climate future forecasts. The IPCC is a large international body responsible for developing reports to provide a scientific basis of the effects of climate change for use in policy and research [40]. The RCPs provide greenhouse concentration projections while the SSPs are a standardized refinement of the RCPs that facilitates comparison between societal choices and subsequent climate change impacts [41]. These forecasts reflect a collection of anticipated climate change effects that include multiple weather parameters. Both the RCPs and SSPs are frequently used in climate change research, e.g., [41–44].

Climate change scenarios, such as those from the IPCC, span a range of severities [40]. Stochastic weather generators utilize a severity as input to generate weather sample paths [45,46]. We adopt the MEWS model due to (i) its ability to generate extreme temperature events by incorporating SSP scenarios, and (ii) its compatibility with other infrastructure models [45]. Other tools were ruled out due to either computational intractability [47] or lack of hourly time-series outputs [48]. The inputs to MEWS include the latitude and longitude of the site, the future analysis years of interest, historical weather data from the National Oceanic and Atmospheric Administration [39], and a historical weather file in Typical Meteorological Year (TMY) format. The outputs are updated weather files for each specified analysis year, which, in turn, serve as input to EnergyPlus, a physics-based model that generates an hourly load profile using building characteristics and hourly weather as input [49].

Our study considers the IPCC scenarios SSP 2-4.5, SSP 3-7.0, and SSP 5-8.5 [41]. The radiative forcing levels (4.5 W/m^2, 7.0 W/m^2, and 8.5 W/m^2) of the RCPs are the important variation for this study. These values represent current goals to keep temperature increase below 1.5 °C all the way to the worst case future available with 5 °C global mean temperature rise from the pre-industrial (1850–1900) mean. We have therefore omitted combinations of RCP with SSP 1 and 4 because they would be redundant for this study. Each of the scenarios run were sampled on 5%, 50%, and 95% probability thresholds for heat wave increase in frequency and intensity [45]. In this study, the future for extreme heat therefore spans from very low amplification of heat waves for medium increases in radiative forcing (i.e., 4.5 W/m^2 at 5% heat wave amplification levels) to very high amplification of heat waves for high increases to radiative forcing (i.e., SSP 8.5 W/m^2 at 95% heat wave amplification).

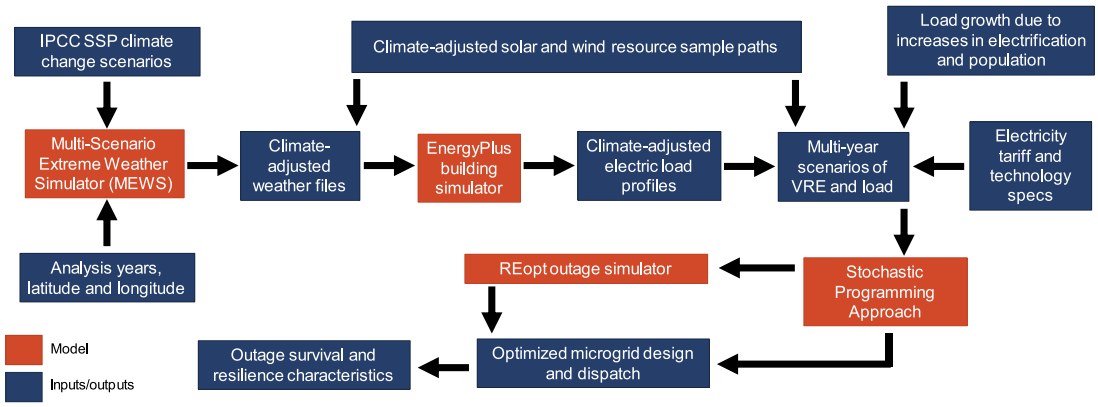

Fig. 1. Flowchart detailing the methodology in this paper.

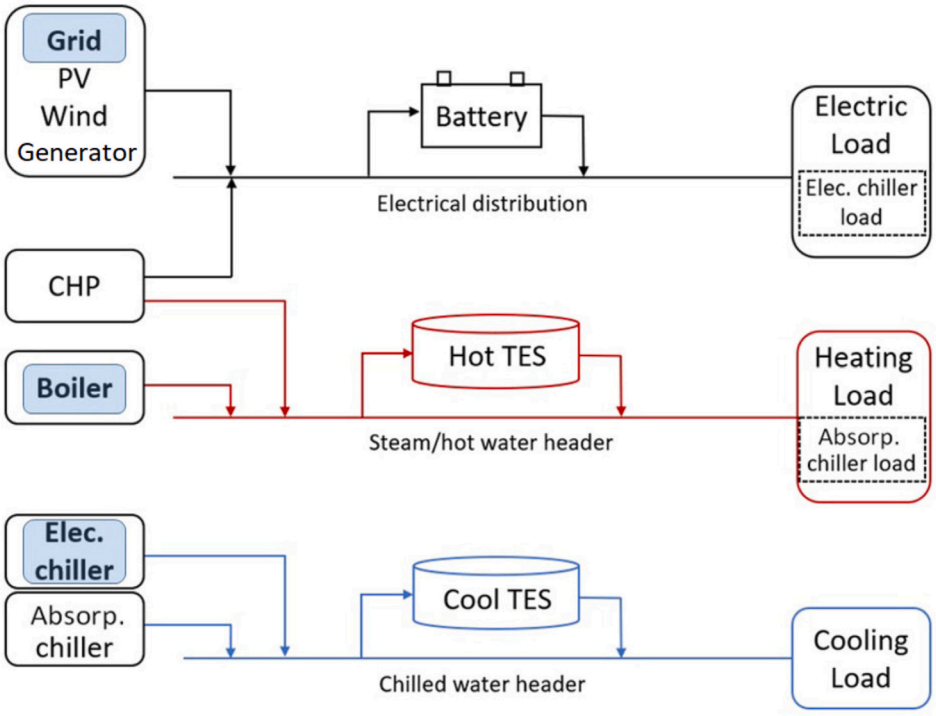

Fig. 2. Schematic detailing the loads served or generated by each technology in REopt. Highlighted technologies represent the business-as-usual case for grid-connected operations; when a diesel generator is present, it is only used during outages.
Image source: [14].

MEWS algorithm overview. This section provides an overview of the methods used to generate future HW events in MEWS. Please refer to previous publications or the source code of MEWS for exact details [45, 50–52]. MEWS uses a minimally complex method to create historical distributions of HW and cold snaps. It then extrapolates in creases in frequency and intensity of HW. Cold snaps are kept at historical levels due to lack of information on how frequency and intensity will change.

A HW event in MEWS consists of: (1) a start time determined by a stochastic transition matrix, (2) a duration determined by a stochastic transition matrix, (3) a duration normalized peak temperature change ΔT distribution above the climate normal temperature distribution's 50th percentile, (4) a distribution of total change in energy ΔE above the climate normal energy distribution's 50th percentile, and (3) a sinusoidal shape function whose parameters equate to randomly sampled *DeltaT* and *DeltaE* to provide a diurnal pattern to the HW event. The complete model contains 14 parameters that are determined by an genetic optimization algorithm which minimizes the difference between the MEWS model's sample distribution and historical HW and cold snap event durations. This fit is conducted for each month of the year, $m = \{1, 2, \ldots, 12\}$. The distributions for ΔE and ΔT are truncated Gaussian distributions which introduce 2 parameters each to the MEWS model. The bounds of these distributions are initially the historic most extreme events and are linear functions of the shift in mean and standard deviation parameters for a given future analysis year.

The 3 × 3 state transition stochastic matrix on the right-hand side of Eq. (1) contains the remaining 10 parameters of the MEWS model:

$$M_m(\Delta t) = \begin{bmatrix} 1 - P_{hw,m} - P_{cs,m} & P_{cs,m} & P_{hw,m} \\ 1 - P_{s_{cs,m}}(\Delta t) & P_{s_{cs,m}}(\Delta t) & 0 \\ 1 - P_{s_{hw,m}}(\Delta t) & 0 & P_{s_{hw,m}}(\Delta t) \end{bmatrix} \quad (1)$$

The first, second, and third rows indicate no wave event, a cold snap event (i.e., cs), and a HW event (i.e., hw), respectively. The first row of the transition matrix is time-invariant, while the other rows depend on

Δt, the time (in hours) since a wave event began. The subscripts cs and hw are represented by the "wave" index $w = \{cs, hw\}$. The $P_{s_{w,m}}(\Delta t)$ functions have a functional form illustrated in Fig. 3, in which:

- $P_{0_{w,m}}$ is the initial probability of sustaining a wave;
- $\Delta t_{p_{w,m}}$ is the time to peak probability $P_{max_{w,m}}$ for an event;
- $P_{max_{w,m}}$ is the maximum probability of remaining in an event; and,
- $\Delta t_{c_{w,m}}$ is the maximum event time.

The temporary increase of this function and subsequent decay provide better fits to the durations of historical wave events, which rarely exhibit immediate decay. This model can be shifted to reflect future conditions by using the procedure found in Villa et al. [45]. The fitted models are then sampled to produce a collection of HW and cold snap events with known durations. The duration-normalized truncated Gaussian distributions are then sampled to produce the temperature change and total energy associated with each event. These samples are used to algebraically constrain the sinusoidal shape function in Eq. (2), which is algebraically fit to the sampled total energy and peak temperature by event:

$$\Delta T(t, D, \Delta t_{min}) = \begin{cases} A \sin\left(\frac{\pi t}{D_{odd}}\right) + B\left(1 - \cos\left(\frac{2\pi t}{\Delta t_{min}}\right)\right) + C & t \le D_{odd} \\ B\left(1 - \cos\left(\frac{2\pi t}{\Delta t_{min}}\right)\right) + C & t > D_{odd}, \end{cases} \tag{2}$$

in which the terms A, B, and C are determined to ensure that the total energy, and peak temperature constraints are satisfied when the energy and temperature truncated Gaussian distributions are sampled. The parameter D_{odd} is the largest odd multiple of Δt_{min} that is less than the HW event duration, D, as shown in Eq. (3):

$$D_{odd} = \Delta t_{min}\left[\left\lfloor \frac{D}{\Delta t_{min}} \right\rfloor - \delta\left(\left\lfloor \frac{D}{\Delta t_{min}} \right\rfloor \mod 2\right)\right]. \tag{3}$$

Here, mod is the modulus operator, $\lfloor\rfloor$ indicates the floor function or closest integer less than the input, and δ is the Dirac delta function. Using D_{odd} instead of D in Eq. (2) avoids erratic variations in the maximum temperature condition with respect to the Heat Wave (HW) duration, enabling mapping ΔT to sampled values from the truncated Gaussian distributions for temperature and energy. After obtaining wave event durations and peak temperatures, MEWS produces time-series weather instances at hourly fidelity that are then provided as input to EnergyPlus to obtain electrical load profiles in our methodology.

2.2. Variable renewable energy

Climate change has implications for the supply side in addition to the demand side of energy systems [53]. Methods for projecting VRE forecasts and trends at various resolutions and time periods include artificial intelligence and machine learning models as seen in Azad et al. [54], forecast combination and ensemble forecasting such as that in Nowotarski et al. [55], day-ahead forecasts, hierarchical forecasting which is implemented in Hyndman et al. [56], and probabilistic forecasting demonstrated in Möhrlen et al. [57], all of which are best-suited for short- to medium-term projections at hourly resolution. This study is concerned with long-term, hourly VRE forecasts which do not exist on the scale in which we are interested. Instead, we consider annual long-term VRE trend projections using large general circulation models that project weather forecasts as an interaction between the atmosphere and the environment as demonstrated in the papers reviewed in Craig et al. (2018) [58].

Craig et al. (2022) [59] note that there is little interaction between climate modeling and energy system modeling efforts, and call for greater inclusion of the former when developing the latter. This paper responds to this call by incorporating a range of anticipated effects of climate change on wind and solar resource. We use the minima and maxima of reviewed projections to represent the range of anticipated effects of climate change on wind resource [58]. Data is extracted for the region most applicable to each case study, from which we calculate a per-year percent change in VRE resource to account for the difference between the publication year and the analysis year. The collection of projections from the literature failed Kolmogorov–Smirnov tests for normal and gamma distributions in each case and there was no intersection between projected ranges in the literature, so we adopt a uniform distribution for the relative resource change per year, in which the range is that of the relevant studies in the literature. Then, for each scenario-year pair, we select a year at random from the available historical weather records [60,61], and we draw independent samples from the uniform distribution to obtain a growth factor which we apply to each time period. As a result, the VRE profiles maintain the same shape as the historical year-long weather profiles we draw from, but have an adjusted magnitude. These altered solar and wind profiles then replace the relevant weather measures in the climate-adjusted weather profiles generated by MEWS to serve as input to the load and VRE models.

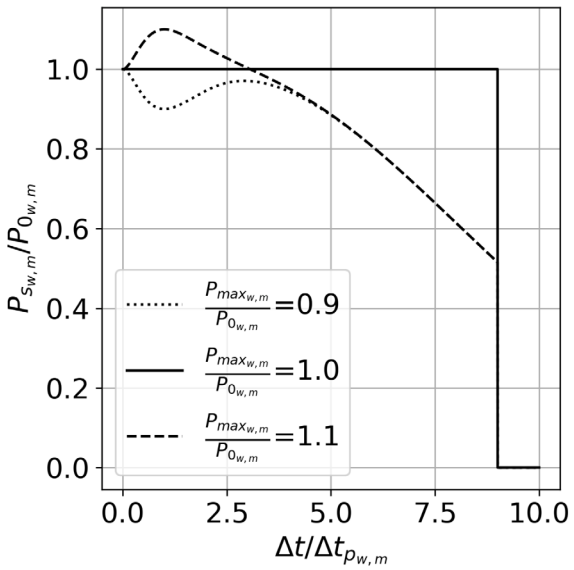

Fig. 3. Probability decay function normalized by the initial probability of sustaining a wave as a function of time elapsed, Δt. $P_{0_{w,m}}$, $P_{max_{w,m}}$, $\Delta t_{p_{w,m}}$, and $\Delta t_{c_{w,m}}$ denote the initial probability, the peak probability, the time to peak probability, and the maximum time associated with sustaining a wave event, respectively.
Image source: [45].

2.3. Multi-year load growth

While individual buildings may not be subject to the same planned growth that regional grid operators plan for, it is important for load profiles of campus-sized microgrids that grow with the local population to capture uncertainties associated with population and electrification increases that may results in fluctuations in load to avoid shortages in future years [17]. Most microgrid design and analysis works in the literature do not consider future loads, and instead use current loads that are assumed to repeat over the project lifetime. The studies that do consider long-term load growth in energy system design analyses design do so for rural microgrids [62,63]. In instances where site-specific data was not available, we adopt a similar methodology to that implemented in Bhattacharyya et al. [63] and Kumar et al. [62] that was applied to rural microgrids. Kumar et al. and Bhattacharyya et al. use historical electrification data to populate their load growth assumptions, while we use historical population data as we assume

the campus is already grid-connected. For the nearest future year, a random variate is generated from a triangular distribution, under the assumption that we have a best guess and range of estimated growth in the shorter term. For all future years, we assume a range but no best guess, and so a random variate is generated from a uniform distribution to represent growth from one period to the next. The product of these inter-period growth factors is applied to each hour of the load profile for each scenario-year pairing obtained via the methodology in Section 2.1.

2.4. Optimization model

This section summarizes our augmentation of REopt to consider multiple scenarios; the solution method we adopt is visualized in Fig. 4; here, $\omega = (m, n)$ denotes a scenario-year pairing of year m and scenario n; X^{ω} denotes the optimal system design for scenario-year pairing ω after accounting for penalties when obtaining a lower bound on the optimal expected lifecycle cost, $z^{\hat{P}}$; and, $\hat{X}$ is the fixed system design when obtaining an upper bound on the expected optimal lifecycle cost, $z^{\underline{P}}$. New solutions are assessed and penalties are updated until the lower and upper bounds are within the optimality threshold, ϵ. We develop lower and upper bound formulations of REopt, separated by uncertainty-informed scenarios. Our extension of REopt outputs an optimal system design and dispatch as well as the expected Life-Cycle Cost (LCC) of the system. Because load and VRE resources are assumed to be uncertain, and the single chosen design must meet the load under any given scenario while minimizing expected lifecycle costs, we formulate the problem as a two-stage stochastic program in which the first stage consists of the size of each generating technology and storage system in the design, and the second stage includes scenario-specific dispatch decisions that depend on both the system sizes in the first stage and the VRE availability and load for each scenario in the second stage. Solving the lower bound formulation outputs unique optimal system designs for each scenario; the designs may differ from scenario to scenario in the lower bound model, subject to a penalty in the objective function. The results of the lower bound are used to select a candidate fixed design for the upper bound formulation. If the ratio between the optimal objective values of the lower and upper bound formulations is not less than the optimality threshold, a bisection search is employed to improve the upper bound, fixed candidate design. Once the optimality threshold condition is satisfied, we explore the other REopt outputs such as the probability of survival and resilience by time step resilience metrics to assess the quality of the solutions produced by our methodologies.

The model we develop seeks microgrid design and operations decisions that minimize expected total LCC of the energy system across a finite collection of scenarios which we generate using the methodology in Section 2. We include a term for unmet load to ensure relatively complete recourse. Additionally, we include boundary conditions to rectify storage inventory and ensure year-to-year continuity. We present the model below in a general form using constructs that highlight the scenario-year pairings and the decomposition method that we employ to obtain upper and lower bounds on optimal expected lifecycle cost.

Our abstraction of REopt resembles the methods employed in [64]. Because the notation in this model, even in its compressed form, is significant, we adopt the notational conventions described in Teter et al. [65] for complex optimization models and summarize the notation in tabular form before describing our formulations in this section, using capital letters to denote variables, lowercase letters to denote indices, functions, or parameters, superscripts to denote either relevant sets to a function or scenario-year pairings, and subscripts to denote indices within sets. The unabridged formulation of REopt is available in Appendix A, and a mapping of decision variables from the general form below and the fully descriptive formulation is available in Appendix B.

2.4.1. Formulation: Stochastic program ($\mathcal{P}$)

Sets		
$h \in \mathcal{H} = \{1, 2..., \lvert\mathcal{H}\rvert\}$	Time periods, (i.e., hours, $\lvert\mathcal{H}\rvert = 8760$)	
$\omega \in \Omega = \{1, 2, ..., \lvert\Omega\rvert\}$	Scenario-year pairs	
$X \in \mathcal{X}$	Strategic design decisions (i.e., system sizes)	
$Y_h^{\omega} \in \mathcal{Y}_h^{\omega}(X)$	Operational (e.g., dispatch) decisions made in time period h and scenario-year ω given decision X	
$W^{\omega} \in \mathcal{W}(Y_1^{\omega}, \ldots, Y_{\lvert\mathcal{H}\rvert}^{\omega})$	Long-term operational decisions made in time period h and scenario-year ω given operational decision Y_h^{ω}	
Parameters		
B_0^{ω}	Initial inventory in scenario-year ω	
ρ^{ω}	Relative weight applied to scenario-year ω	[fraction]
Functions		
$f^X(\cdot)$	Cost of a design decision	[$]
$f^Y(\cdot)$	Cost of an operational decision	[$]
$f^W(\cdot)$	Cost of long-term operational decisions	[$]
$f^V(\cdot)$	Cost of unmet load associated with the unmet load V_h^{ω}	[$/kW]
$\ell_h^{\omega}(\cdot)$	Unmet load associated with operational decision in time period h and scenario-year ω	[kW]
$b_h^{\omega}(\cdot)$	Net change in storage inventory associated with operational decision in time period h and scenario-year ω	
Decision variables		
X	Design decision	
X^{ω}	Design decision associated with scenario-year ω	
Y_h^{ω}	Operational decision made in time period h and scenario-year ω	
W^{ω}	Long-term operational decision made in scenario-year ω	
V_h^{ω}	Unmet load in time period h and scenario-year ω	[kW]
B_h^{ω}	Storage inventory at the end of time period h in scenario-year ω	
W^{ω}	Operational decisions in scenario-year ω	

Formulation ($\mathcal{P}$)

$$\text{minimize } z^{\mathcal{P}} = \sum_{\omega \in \Omega} \rho^{\omega} \left[f^X(X^{\omega}) + \sum_{h \in \mathcal{H}} \left[f^Y(Y_h^{\omega}) + f^V(V_h^{\omega}) \right] + f^W(W^{\omega}) \right] \quad (4a)$$

$$\text{s.t.} \quad X^{\omega} \in \mathcal{X} \ \forall \ \omega \in \Omega \quad (4b)$$

$$Y_h^{\omega} \in \mathcal{Y}_h^{\omega}(X^{\omega}) \ \forall \ h \in \mathcal{H}, \ \omega \in \Omega \quad (4c)$$

$$W^{\omega} \in \mathcal{W}(Y_1^{\omega}, \ldots, Y_{\lvert\mathcal{H}\rvert}^{\omega}) \ \forall \ \omega \in \Omega \quad (4d)$$

$$V_h^{\omega} = \ell_h^{\omega}(Y_h^{\omega}) \ \forall \ h \in \mathcal{H}, \ \omega \in \Omega \quad (4e)$$

$$B_h^{\omega} = B_{h-1}^{\omega} + b_h^{\omega}(Y_h^{\omega}) \ \forall \ h \in \mathcal{H} \backslash \{1\}, \ \omega \in \Omega \quad (4f)$$

$$B_1^{\omega} = B_0^{\omega} + b_1^{\omega}(Y_1^{\omega}) \ \forall \ \omega \in \Omega \quad (4g)$$

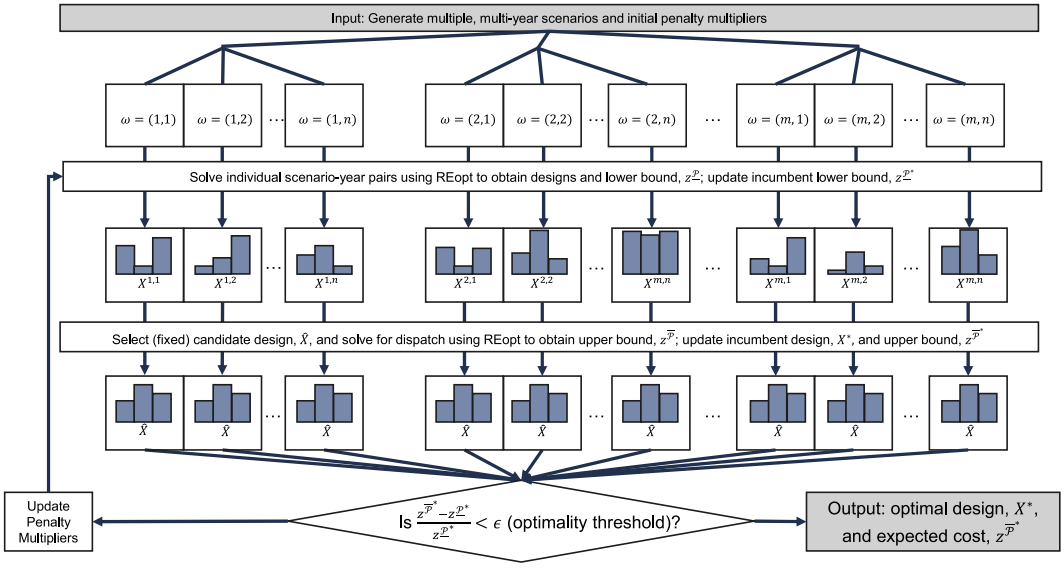

Fig. 4. Graphical description of information flow in our two-stage stochastic programming method, adapted from [64]. Here, $\omega = (m, n)$ denotes a scenario-year pairing of year m and scenario n; X^{ω} denotes the optimal system design for scenario-year pairing ω after accounting for penalties when obtaining a lower bound on the optimal expected lifecycle cost, z^{P}; and, $\hat{X}$ is the fixed system design when obtaining an upper bound on the expected optimal lifecycle cost, $z^{\overline{P}}$. New solutions are assessed and penalties are updated until the lower and upper bounds are within the optimality threshold, ϵ.

$$B^{\omega}_{|\mathcal{H}|} = B^{\omega}_{0} \;\forall\; \omega \in \Omega \tag{4h}$$

$$X^{\omega} = X \;\forall\; \omega \in \Omega \;:\; \mu^{\omega} \tag{4i}$$

In the objective of model (4a), we seek a minimum expected LCC, which composed of the fixed cost of procuring the microgrid design and the expected value of operational decisions over the operating horizon. The weight applied to each scenario-year pair, ρ^{ω}, assumes equal-probability and a time-specific discount factor in future years. Constraint (4b) specifies feasible design decisions, including constraints on the maximum system size to obtain net metering benefits and limits on individual system capacities. Constraint (4c) specifies feasible operational decisions given the design decision X for all time periods in each scenario, including the power output of each technology and any utility purchases to meet the site load in each time step; for example, the power output of a diesel generator may not exceed its capacity. The variable Y^{ω}_{h} is defined for each scenario-year and time step to account for production factors and loads that vary by time period and scenario. On the other hand, parameters such as monthly demand charges and aggregated production incentives do not vary on an hourly basis and are considered multi-period costs. As a result, W^{ω} is introduced to capture the costs that vary only by scenario-year ω, as defined in constraint (4d). Constraint (4e) defines the amount of unmet load V^{ω}_{h} as the unmet load associated with an operational decision Y^{ω}_{h} for each time period in each scenario. The unmet load variable, V^{ω}_{h}, is not defined in the existing REopt model. Therefore, this formulation adds this variable V^{ω}_{h} is defined in Eq. (5). Eq. (5) is written adopting the original REopt notation, as outlined in Hirwa et al. [66].

$$\begin{aligned} \underbrace{V^{\omega}_{h}}_{\text{unmet load}} = \underbrace{\delta^{\mathrm{d},\omega}_{h}}_{\text{site load}} - \underbrace{\sum_{t\in\mathcal{T}} f^{p}_{th}\cdot f^{l}_{t}\cdot X^{rp}_{th}}_{\text{DER production}} \\ - \underbrace{\sum_{b\in B^{e}} X^{dfs}_{bh}}_{\text{battery discharge}} - \underbrace{\sum_{u\in U^{*p}} X^{g}_{uh}}_{\text{grid purchase}} + \underbrace{\sum_{t\in\mathcal{T}^{e}/\mathcal{T}^{g}}\sum_{b\in B^{e}} X^{pts}_{bth}}_{\text{battery charged by mircogrid}} \\ + \underbrace{\sum_{t\in\mathcal{T}^{e}/\mathcal{T}^{g}}\sum_{u\in U^{s}_{t}} X^{ptg}_{tuh}}_{\text{production sold to grid}} + \underbrace{\sum_{u\in U^{*sb}} X^{stg}_{uh}}_{\text{battery charged by grid}} \\ \forall\; h\in\mathcal{H},\; \omega\in\Omega \end{aligned} \tag{5}$$

From left to right, the unmet load is equal to the (1) site load minus (2) power produced by DERs, (3) power discharged from storage, and (4) power purchased from the grid, plus the (5) power delivered to charge storage and (6) power sold to the grid from DER production and storage for each hour in each scenario-year pairing. The defined notation for this constraint can be found in Hirwa et al. [66] and Appendix A. Constraint (4f) balances battery state of charge B^{ω}_{h} between consecutive time periods while constraint (4g) provides an analogous restriction on inventory to constraint (4f) for the first time period according to initial inventory conditions, B^{ω}_{0}. To ensure year-to-year continuity, constraint (4h) balances storage inventory. Constraint (4i) enforces the nonanticipativity of X^{ω} which prevents the strategic design decisions from adapting to individual scenarios.

2.4.2. Formulation: Lower bound ($\underline{P}$)

Model ($\underline{P}$) is intractable when solved directly using an off-the-shelf solver. However, removing constraint (4i) from the formulation, separates the model naturally by scenario-year pair. Our relaxation of model (P), which we call ($\underline{P}$), moves this constraint into the objective function, which allows the resulting scenario-year-specific sub-models to be solved in parallel. The lower bound model allows for the microgrid generator and storage sizes to be different for each scenario-year pair, subject to the penalty, μ, which we vary by

Formulation ($\underline{P}$)

$$\begin{aligned} \text{minimize} z^{\underline{P}} = \sum_{\omega\in\Omega}\rho^{\omega}\Big[f^{X}(X^{\omega}) + \sum_{h\in\mathcal{H}}\big[f^{Y}(Y^{\omega}_{h}) + f^{V}(V^{\omega}_{h})\big] \\ + f^{W}(W^{\omega}) + \mu^{\omega}(X^{\omega} - X)\Big] \\ \text{s.t.} \quad (4b)\text{–}(4h) \end{aligned} \tag{6a}$$

In the lower bound formulation ($\underline{P}$), we take the Lagrangian relaxation of (4i) and the term $\sum_{\omega\in\Omega}\mu^{\omega}(X^{\omega} - X)$ is moved to the objective function. We require $\sum_{\omega\in\Omega}\mu^{\omega} = 0$ to prevent the problem from becoming unbounded, as the restriction on X is removed. This is consistent with the progressive hedging method developed by Rockefellar and Wets [67], but we remove the proximal term to ensure that model ($\underline{P}$) is a relaxation of model ($\underline{P}$) [68]. As a result, the optimal objective value of model ($\underline{P}$) provides a lower bound to that of model (P), i.e., $z^{\underline{P}} \le z^{P}$.

2.4.3. Formulation: Upper bound ($\bar{\mathcal{P}}$)

While model $\underline{\mathcal{P}}$ provides a lower bound of model ($\mathcal{P}$) an upper bound is still needed, i.e. a restriction of model ($\mathcal{P}$). This is achieved in model ($\bar{\mathcal{P}}$). In this formulation, we fix X to a single strategic design decision, making it a feasible solution to model ($\mathcal{P}$). The resulting formulation, model $\bar{\mathcal{P}}$, is a restriction and upper bound of model $\mathcal{P}$.

Additional parameter

$\hat{X}$	Strategic design decision

Formulation ($\bar{\mathcal{P}}$)

$$\text{minimize } z^{\bar{\mathcal{P}}} = f^X(\hat{X}) + \sum_{\omega\in\Omega} \rho^\omega \Big[\sum_{h\in\mathcal{H}} \big[f^Y(Y_h^\omega) + f^V(V_h^\omega) \big] + f^W(W^\omega) \Big] \quad (7a)$$

$$\text{s.t.} \quad Y_h^\omega \in \mathcal{Y}_h^\omega(\hat{X}) \;\forall\, h \in \mathcal{H},\ \omega \in \Omega \quad (7b)$$

(4e)–(4h)

The objective function (7a) is adjusted to specify a singular, fixed design decision such that $\hat{X} = X \in \mathcal{X}$. The fixed design also enabled for the removal of constraint (4i) and the nonanticipativity term from the objective. As a result of the fixed design, model ($\bar{\mathcal{P}}$) is a restriction of ($\mathcal{P}$). The optimal solution to $\bar{\mathcal{P}}$ will provide an upper bound to the optimal value of ($\mathcal{P}$), i.e., $z^{\bar{\mathcal{P}}} \geq z^{\mathcal{P}}$.

2.4.4. Solution methods

We solve models ($\underline{\mathcal{P}}$) and ($\bar{\mathcal{P}}$) to obtain lower and upper bounds, respectively, on the objective value of model ($\mathcal{P}$). By first solving each scenario-year-specific submodel in model ($\underline{\mathcal{P}}$) with penalties $\mu^\omega = 0,\ \forall\omega \in \Omega$, we can obtain up to $|\Omega|$ candidate (fixed) designs, which we can assess by solving model ($\bar{\mathcal{P}}$). We can update the penalties, μ^ω, using progressive hedging [67] to refine the lower and upper bounds as needed until the optimality criterion for a case is met, and we can further improve the upper bound using a multi-dimensional bisection search [69] due to the continuous domain and relatively small number of design decisions.

2.5. Resilience assessment

In addition to understanding the effects of our methods on system sizing and dispatch decisions, we are also concerned with its effects on the climate resilience of the system. Within REopt, a microgrid or DER planner can evaluate the resilience of their microgrid system with the outage simulator [18,66,70]. This tool details the amount of time a system can continue to meet the critical load throughout the year with probability of survival and expected resilience by time step metrics. Every hour, the outage simulator calculates how many hours the on-site system can meet the critical load (probability of survival) and the duration of survival for outages starting at each hour of the year (expected resilience by time step) [14]. These metrics are built into the REopt outage simulator [71] and are described in Section 4.6 from Hirwa et al. [66]. This feature can also assess expected microgrid system performance and costs under user-specified grid outages. This study explores the resilience of our systems optimized with and without consideration of outages.

In addition, we calculate the Area Under the Curve (AUC) metric from Sepúlveda-Mora and Hegedus [22], as demonstrated in Eq. (8):

$$AUC_N = \sum_{t=1}^{N} P\ (\text{surviving an outage of } t \text{ hours}) \cdot (1\text{ h}). \quad (8)$$

This metric can capture uncertainty across many time periods and requires minimal data that is generally needed for Value of Lost Load (VoLL)-based or composite indicator resilience metrics [72]. To calculate this metric, the probability of survival from the REopt outage simulator is used to populate the function. Additionally, the quotient of a the AUC_N and N represents the probability of the system surviving an outage of duration 1 to N that starts at a random time step.

2.6. Stochastic metrics

We utilize metrics from the stochastic programming literature to assess the quality of solutions that we obtain using the methodology described in Section 2.4. Similar to the notation implemented in [73], we refer to the solution to model ($\mathcal{P}$) via the methods in Section 2 as the Recourse Problem (RP) solution. The first metric is the Expected Value of the Stochastic Solution (EVSS) which justifies the application of the stochastic model by comparing the RP solution to an alternative, single-scenario instance that uses the expected value of each random variable as input, which we refer to as the EV problem. The EVSS is the difference between the expected LCC of the EV design under a collection of Out-of-Sample (OOS) scenarios, z_{EV}, and that of the RP design, z_{RP}, as demonstrated in Eq. (9):

$$EVSS = z_{RP} - z_{EV}. \quad (9)$$

We can further assess solution quality by performing an out-of-sample validation to obtain a valid confidence interval of the optimality gap, using the Sample Average Approximation (SAA) method from Mak et al. [19]. The calculation of this metric is shown in Eqs. (10) and (11):

$$\bar{z} = \sum_{k\in K} \rho^k (z_{RP}^k - z_{LB}^k) \quad (10)$$

$$\bar{\varepsilon} = \frac{t_{\alpha,n-1}\, s(n)}{\sqrt{n}}, \quad (11)$$

in which:

- z_{RP}^k and z_{LB}^k are the lifecycle costs of the solution using the RP design and the lower-bound model allowing a free design for each scenario-year pair, respectively, for out-of-sample scenario k;
- $s(n)$ is the sample standard deviation for the differences $z_{RP}^k - z_{LB}^k$, $k \in \{1, \ldots, n\}$;
- $\rho^k = 1/n,\ \forall k \in \{1, \ldots, n\}$; and,
- $t_{\alpha,n-1}$ is the t-statistic inverted at α with $n-1$ degrees of freedom.

Using this framework, the $(1-\alpha)$-level confidence interval on the optimality gap is $[0, \bar{z} + \bar{\varepsilon}]$.

3. Results

3.1. Case study descriptions

Table 1 summarizes key inputs for the two sites chosen for case studies: Albuquerque, New Mexico and Kodiak, Alaska. Each case study assumes default costs available in REopt [71] but includes a capital cost multiplier for purchased technologies in Kodiak due to its remote location. These locations are unique in climate and VRE availability, as demonstrated in Fig. 5. Historical VRE data was collected for both locations going back to 1998. The annual average wind and Photovoltaic (PV) capacity factors for all collected years are visualized in Fig. 5 and exhibit disparate VRE profiles for the two case studies. Additionally, the summary of (i) daily high and low temperatures and (ii) annual precipitation for Kodiak and Albuquerque, shown in Table 1, further illustrate the difference in climate between the two case studies. For both case studies, we model present day, 2035, and 2050. For the Kodiak case, we developed a multi-building campus load informed by total energy usage and peak demand on a monthly basis provided by a partner. We assume an office building for Albuquerque because no further site-specific data was provided. The average loads for all present-year scenarios for the Kodiak and Albuquerque cases were approximately 1400 kW and 50 kW, respectively. We fit a weighted collection of the DOE reference commercial building loads [74] to the historical campus load by minimizing the sum of squared error of monthly peak-average ratio of the expected and observed loads, then we scale the hourly load profiles in each month so that the average and peak load of the simulated campus load matches the historical billing

Table 1
Case study inputs.

Location		Kodiak	Albuquerque
Building		Multi-building campus	Medium office
Avg. Hi/Lo Temp.		8 °C/2 °C	21 °C/7 °C
Annual Precip./Snow		127 cm/200 cm	21 cm/25 cm
Load growth scalar	2023	No change	
	2035	[1+Tri(0.15,0.25,0.2)]	1+Tri(0.15,0.19,0.17)
	2050	[1+Tri(0.15,0.25,0.2)] ∗ [1+Uni(0.0,0.2)]	1+Tri(0.15,0.19,0.17) ∗ [1+Uni(0.01,0.15)]
VRE change: PV	2023	No change	
	2035	[−5.5%, 1.8%]	[−0.7%, 0%]
	2050	[−10%, 3.2%]	[−1.3%, 0%]
VRE change: Wind	2023	No change	
	2035	[−10.5%, 0%]	[−7.0%, 7.0%]
	2050	[−18.9%, 0%]	[−12.6%, 11.5%]
Business as usual (BAU) system		No existing generators or storage	
Back-up system		Battery generator	No existing generators or storage
Capital cost multiplier		1.5	1.0
Electricity tariff		Kodiak Electric Assn. Large Power	Public Service Co of NM 2B Small Power Service - TOU
ASHRAE climate zone		6A	4B
Building standard		ASHRAE 90.1-2016	

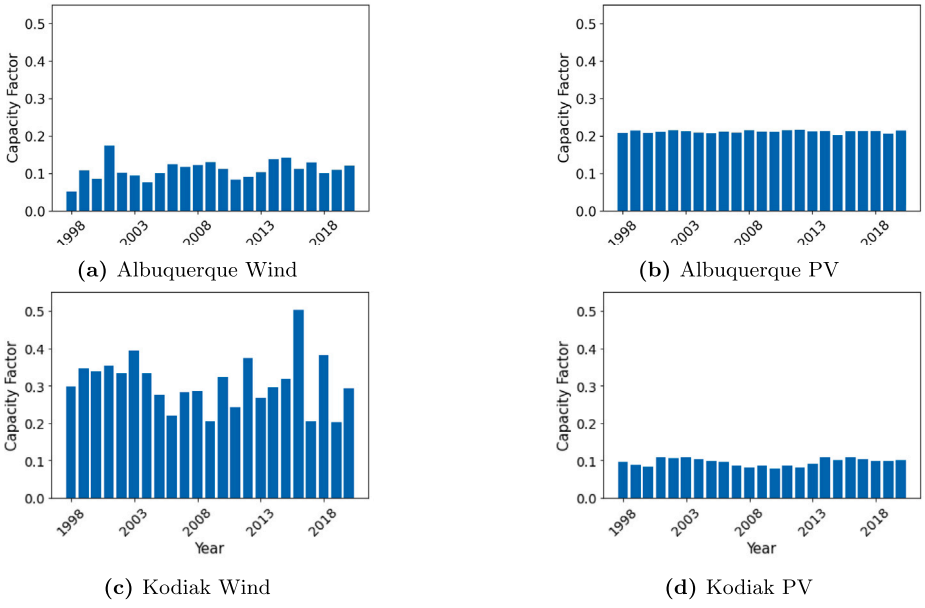

(a) Albuquerque Wind (b) Albuquerque PV

(c) Kodiak Wind (d) Kodiak PV

Fig. 5. VRE capacity factors from 1998–2020.

data exactly. The output of this methodology includes a (i) load profile that replicates historical billing, and (ii) a collection of building energy models that are compatible with the scenario generation methodology in Section 2.

3.2. MEWS results

The MEWS fits for Albuquerque and Kodiak were carried out using climate norms from Albuquerque International Airport (Station USW00023050) from 1931 to 2021 and Seward Airport (Station USW00026438) from 1965 to 2022, respectively. The fits failed to reject a null hypotheses of equal distributions according to the Kolmogorov–Smirnov p-test at $\alpha = 0.05$. For Albuquerque temperature distributions, 75% failed to reject for HW events and 67% for cold snaps. For Albuquerque duration distributions, all but one failed to reject for HW events and 75% passed for cold snaps. The worst-case temperature fit was in July as shown on the top of Fig. 6; the failed p-test is most likely due to the multimodal nature of the historical record due to the time resolution of data collected, and does not require closer fitting. Similar results were observed for Kodiak, as illustrated in the bottom of Fig. 6.

The CMIP6 surface temperature increases for Albuquerque are shown in Fig. 7. The polynomial fits (solid lines) for each SSP were used to produce different future shifts to temperature distributions per the MEWS algorithm as shown in Fig. 8. The future distribution in yellow-orange in Fig. 8 was used to sample new HW and cold snap events on 200 weather files each for the three climate scenarios (SSP2-4.5, SSP3-7.0, and SSP5-8.5), three HW event percentiles (5%, 50%, and 95%), and 3 years (2020, 2035 and 2050). The resulting files contained maximum temperatures of 54.7 °C for Albuquerque and 39.9 °C for Kodiak in 2050. Minimum temperatures in the ensemble were −23.3 °C −38.5 °C for Albuquerque and Kodiak, respectively.

3.3. Microgrid optimization results

All case study instances in this section were solved using the REopt.jl package v0.32 with Xpress version 16.1. Individual scenario-year-specific instances of REopt took less than 30 s each. We adopt a

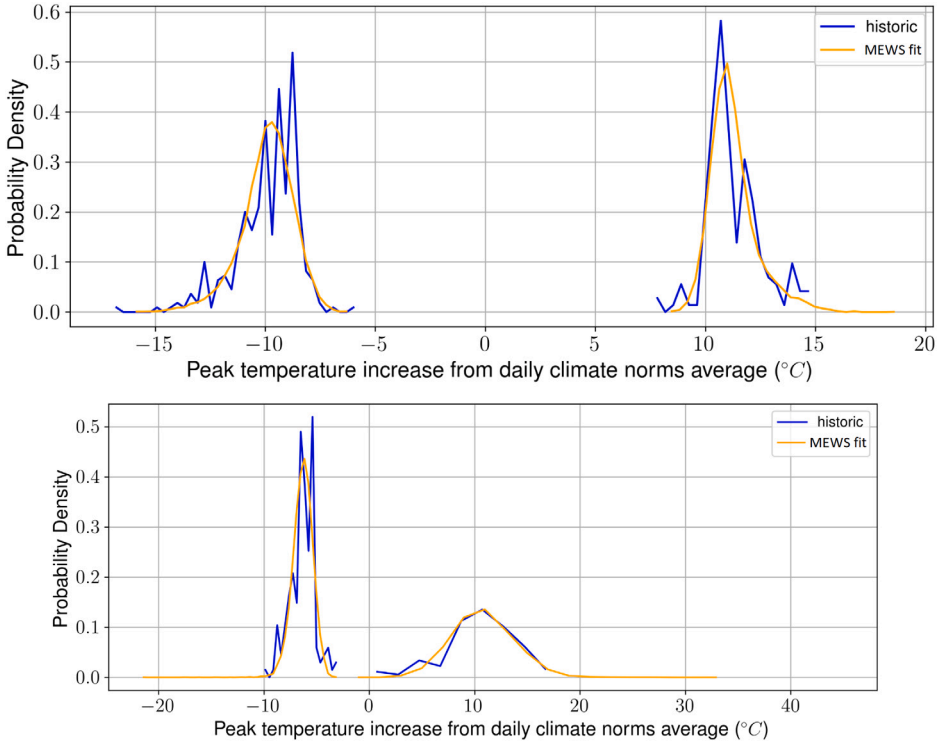

Fig. 6. Worst case month (July) fit for Albuquerque temperatures (top). A similar, multimodal distribution is present for the historical observations for Kodiak in July (bottom).

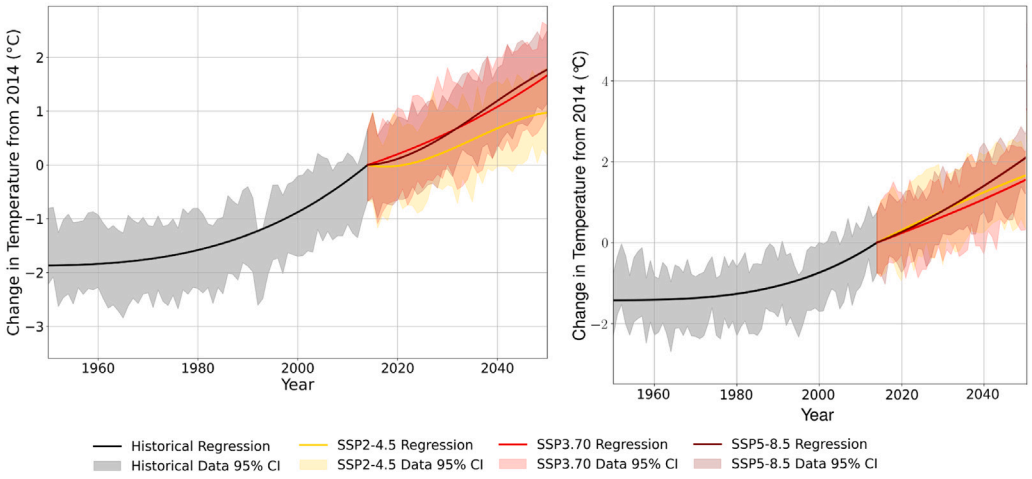

Fig. 7. CMIP6 Surface temperature change for Albuquerque (left) and Kodiak (right).

stopping criterion of obtaining a solution within 5% of optimality to be consistent with other design-and-dispatch papers in the literature [13,64,75,76]; in each case study, this threshold was reached in less than three hours. The recourse problem uses 22 scenarios for each case study while the sample average approximation uses 30 additional scenarios; each scenario spans three analysis years which are solved individually when solving models ($\underline{P}$) and ($\overline{P}$) as part of the methodology in Section 2.4.

Table 2 summarizes the results obtained via the two-stage stochastic programming approach in Section 2.4 for the Kodiak and Albuquerque case studies. Both cases benefit from the addition of renewable DER when compared to the business-as-usual case of purchasing no new assets. The difference in available VRE resources motivates the purchase of wind and PV exclusively for Kodiak and Albuquerque, respectively; storage technologies are not economical in either case. Fig. 9 summarizes the dispatch decisions for a week in August in an example scenario-year pairing for the Albuquerque case study. The PV system is sized to meet the office building load during the week when occupancy is high with limited or no curtailment, and then excess energy production by the PV system on the weekend is curtailed when the site load is low due to a lack of net metering available. While PV productivity and load vary by scenario-year pairing, this trend is consistent by scenario and year.

The high year-to-year variation in the annual average capacity factor of wind in Kodiak (see Fig. 5(c)) yields a much greater EVSS associated with the optimal design when compared to the variation of the annual solar resource in Albuquerque (see Fig. 5(b)). This demonstrates the value of our methodology for cases in which the most economical renewable technology has a highly variable annual production for a microgrid planning model like REopt. This differs from unit commitment and other energy applications in which the operating time window is relatively short and generator decisions are

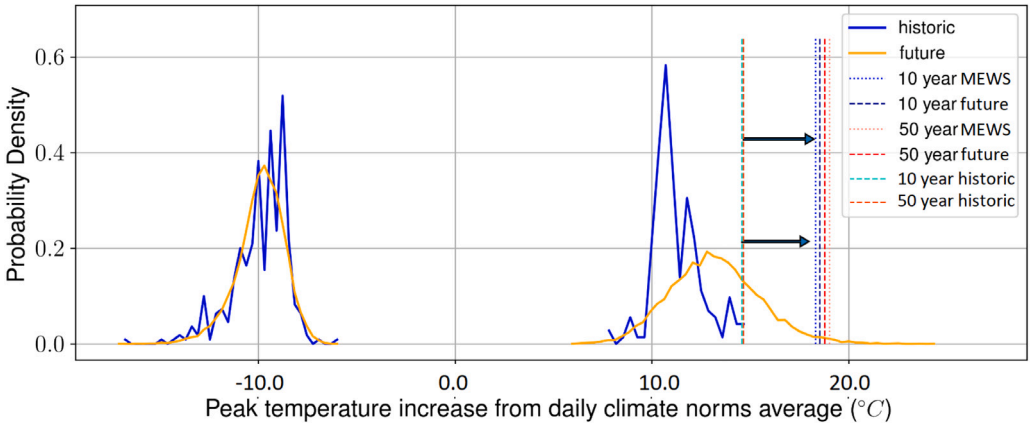

Fig. 8. Illustration of Albuquerque MEWS shift for July SSP5-8.5 95% CI for HW shift and future year 2050.

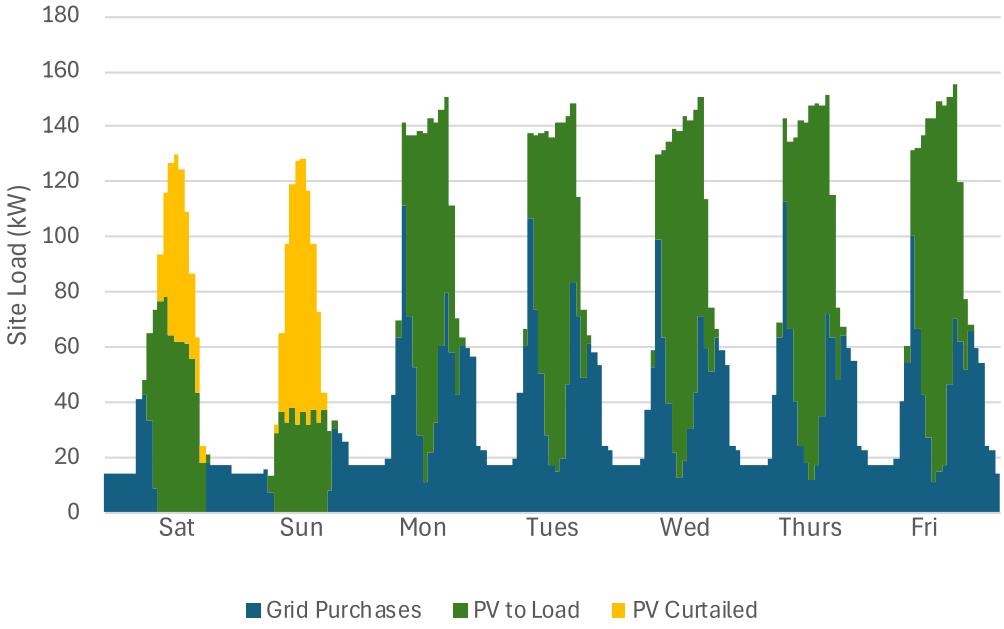

Fig. 9. Example load and electricity dispatch profile for one week in August of a single scenario-year pairing of the Albuquerque case study.

made in a day-ahead or real-time market, and in which VRE changes can have a significant impact on pricing; this phenomenon is likely due to the behind-the-meter nature of our model, in which the pricing from the utility is relatively stable over the course of the year and, in our case, deterministic. The 95% CI on each case study's optimality gap has an upper bound of less than 5%, indicating that the sample sizes employed for the recourse problem were sufficient to provide a high-quality stochastic solution. Fig. 10 summarizes the designs selected for the Kodiak case study as sources of uncertainty are incrementally added and evaluates the expected LCC of each solution using the same out-of-sample validation scenarios as shown in the prior results. The MEWS instance was developed when only considering the anticipated effects of climate-driven extreme temperature events on load growth. The MEWS & PG instance considers the anticipated effects of climate-driven extreme temperature events and population growth on load growth, where "PG" represents population growth. In the MEWS & PG & VRE instance, the anticipated effects of climate-driven extreme temperature events and population growth on load growth as well as a variety of VRE profiles are considered. The RP instance then adds the anticipated effects of climate change on VRE availability in scenario generation. Considering all of the above sources of uncertainty in the scenario generation methodology for the Kodiak case study prevents oversizing the wind turbine, resulting in an improved expected LCC compared to other (incomplete) scenario generation methods.

Table 2
Summary of microgrid designs and expected lifecycle costs under the BAU case of purchasing nothing, and solving the EV (i.e., deterministic) and RP (i.e., model (P)) instances for the Kodiak and Albuquerque case studies.

Result	Kodiak	Albuquerque
BAU LCC [$MM]	23.0	0.771
EV design	Wind: 3057 kW	PV: 189.75 kW
EV LCC [$MM]	24.8	0.602
RP design (X*)	Wind: 855 kW	PV: 179.25 kW
RP LCC [$MM]	22.4	0.601
Expected savings vs. BAU [$MM]	0.573	0.184
EVSS [$MM]	2.4	0.001
95% confidence interval on optimality gap [%]	[0, 4.51]	[0, 0.923]

3.4. Resilience assessment

Figs. 11 and 12 summarize the resilience results for the Kodiak and Albuquerque case studies, respectively. The left sub-figures show the

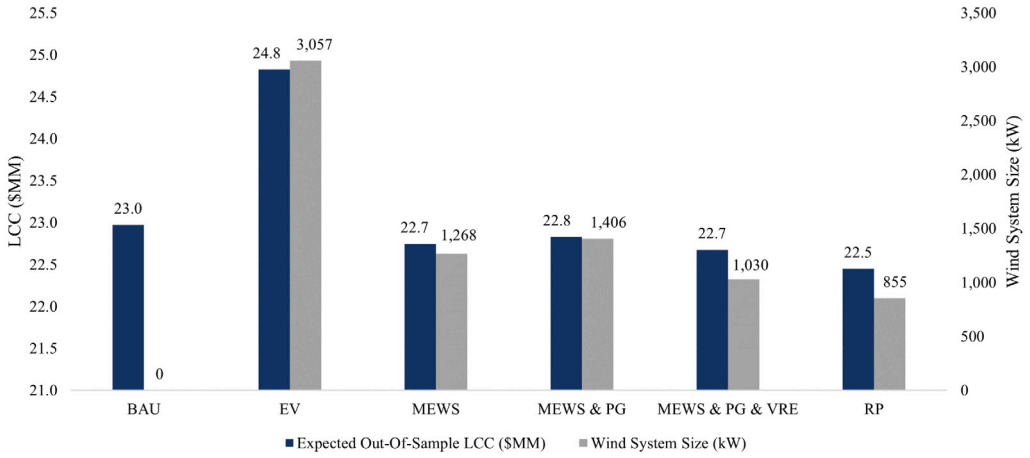

Fig. 10. Summary of expected lifecycle cost and optimal wind system size for the Kodiak case study, as additional sources of uncertainty are added using the methodology in Section 2.

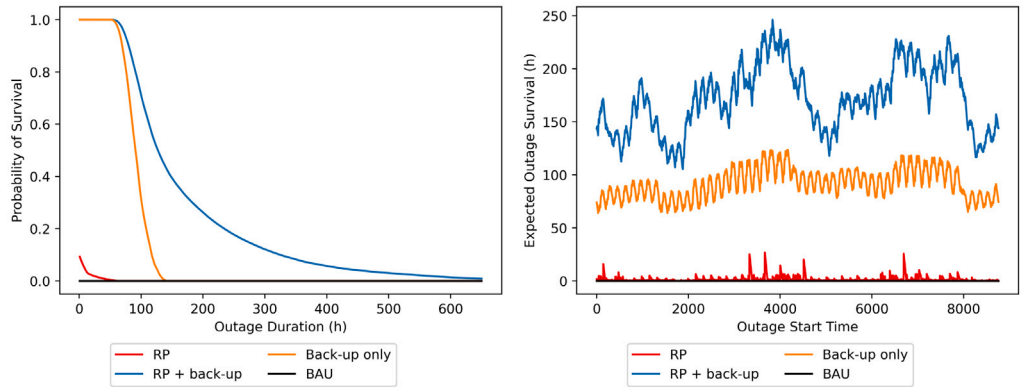

(a) Probability of Survival (b) Resilience by Time Step

Fig. 11. Summary of outage survival statistics, with and without (a) the optimal design obtained by solving model ($\mathcal{P}$), and (b) the assumed existing backup system, for the Kodiak case study.

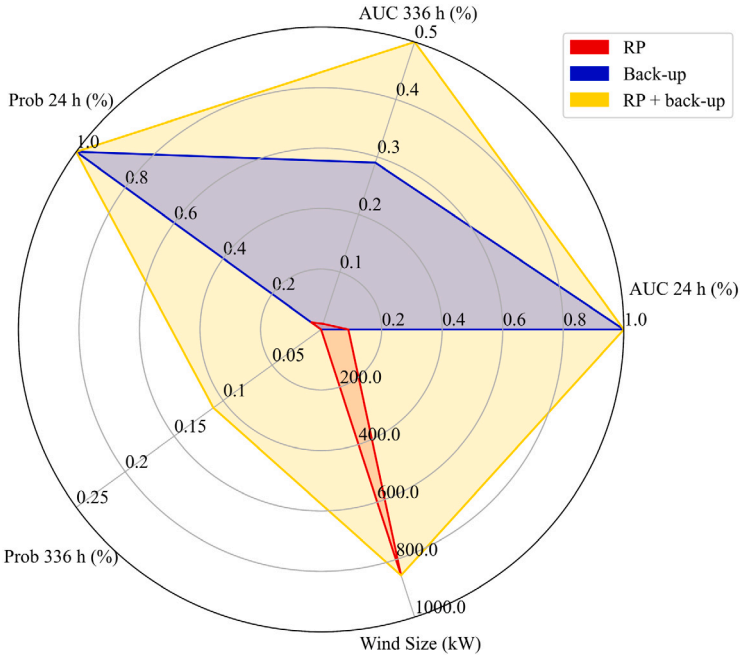

Fig. 12. Summary of outage survival statistics, with and without the optimal design obtained by solving model ($\mathcal{P}$), for the Albuquerque case study.

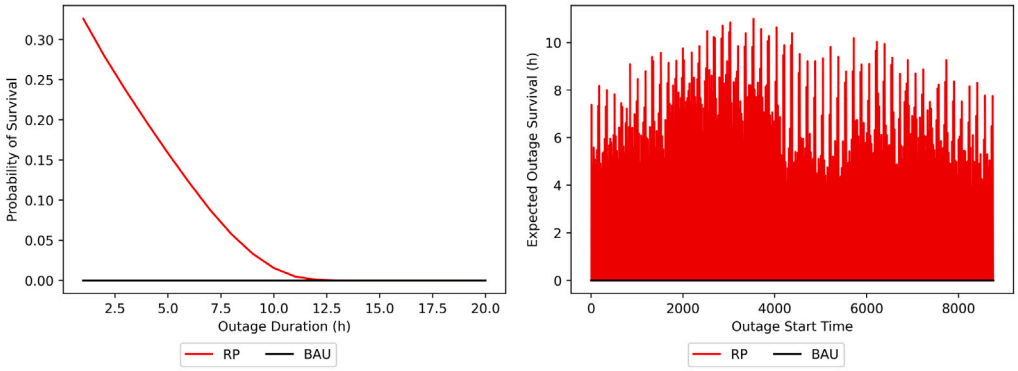

(a) Probability of Survival (b) Resilience by Time Step

Fig. 13. Comparison of resilience metrics for the Kodiak case study with and without (i) the optimal microgrid design obtained by solving model ($\mathcal{P}$), and (ii) the existing backup system. "AUC" represents the $\frac{AUC_N}{N}$ of the specified outage duration and "Prob" represents the probability of survival of the specified outage duration.

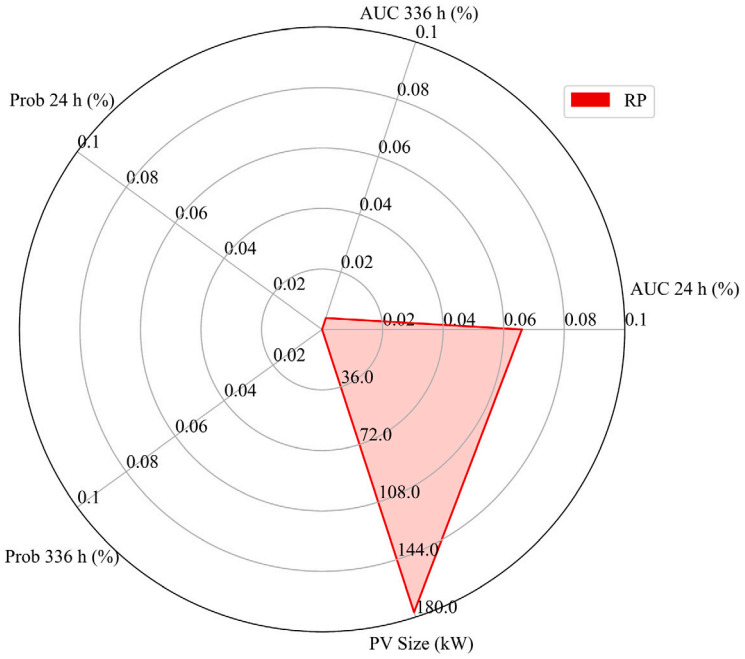

Fig. 14. Comparison of resilience metrics for the Albuquerque case study with the optimal microgrid design obtained by solving model ($\mathcal{P}$). "AUC" represents the $\frac{AUC_N}{N}$ of the specified outage duration and "Prob" represents the probability of survival of the specified outage duration.

probability of survival of a given outage duration, while the right subfigures display the outage survival by time step. The results show that while adding renewable technologies can supplement existing backup infrastructure to significantly extend the outage survival, the intermittency of VRE resources prevent these additional assets from providing backup power in the absence of co-located storage or fuel-fired generators.

Figs. 13 and 14 summarize the resilience metrics described in Section 2.5 for Kodiak and Albuquerque, respectively. For both case studies, the BAU case has a value of zero for all metrics and system sizes. Adding the cost-optimal wind turbine to the Kodiak back-up system increases the AUC of the 336-h outage from 29% to 50% while the probability of survival of a 336-h outage increases from 0% to 11%. The lack of a backup system in the Albuquerque case study explains the limited AUC of a 24-h outage of 6.6% when the cost-optimal PV system is included.

These results demonstrate how our methodology is able to design a system that accounts for the long life of electricity-producing assets and the potential changes in load and VRE resources that may take place for a building or campus over the life of the microgrid. The differences between the Kodiak and Albuquerque case studies highlight that the methodology is best-suited for locations with highly variable and productive VRE resources. Additionally, the resilience measures for the microgrid improve more prominently when it is paired with a back-up storage and/or generator system that may not be economical to purchase when optimizing for expected long-term utility, procurement and operations costs.

3.5. Caveats

While the initial weather files that serve as input to EnergyPlus to generate the load profiles are also that which populate the VRE profiles, the additional adjustments we apply to these profiles as described in Sections 2.2–2.3 are applied independently using separate forecast models, i.e., the adjustments to VRE do not impact the temperature profiles. It would be preferable to directly use a single local, downscaled climate projection model as a source of weather, such as those applied in [77,78] and presented in [79] in the place of scalar multiples

that maintain the shape of the load and VRE profile and only alter magnitude; this is an opportunity for further improvement of our multi-year load and VRE forecasting framework, which we intend to develop in future work.

4. Conclusions and future work

In this paper, we augment an existing microgrid design and dispatch model to consider uncertainties including future load growth, climate change impacts on load, and climate change impacts on VRE availability. Our novel contribution includes a two-stage stochastic programming extension of an existing mixed-integer linear program and a scenario generation methodology that incorporates these sources of uncertainty. We illustrate the value of the methodology by selecting two case studies that vary significantly in climate, VRE availability, and site load. The results show that our methodology is well-suited for sites with high VRE variability, and that adding renewable technologies to an existing backup system can significantly extend the resilience of the site in extended outages.

The methodology that we present is general enough to include the heating and cooling technologies available in REopt, and analysis of co-optimizing design for thermal and electrical loads will be explored in future work. The methodology could also be extended to consider weather-induced outage events in addition to the heat waves and cold snaps provided by MEWS. Applying this methodology on a wider variety of climate zones, building types, and load patterns may help to assess what the cost of additional resilience would be for a given building by including stochastic outages within the optimization, instead of optimizing for cost and then assessing resilience afterward.

CRediT authorship contribution statement

Madeline Macmillan: Conceptualization, Data curation, Formal analysis, Investigation, Methodology, Software, Visualization, Writing – original draft, Writing – review & editing. **Alexander Zolan:** Formal analysis, Investigation, Methodology, Supervision, Validation, Writing – original draft, Writing – review & editing. **Morgan Bazilian:** Conceptualization, Methodology, Supervision, Validation, Writing – review & editing. **Daniel L. Villa:** Data curation, Methodology, Software, Validation, Visualization, Writing – original draft, Writing – review & editing.

Declaration of competing interest

The authors declare that they have no known competing financial interests or personal relationships that could have appeared to influence the work reported in this paper.

Data availability

The authors do not have permission to share data.

Acknowledgments

This paper was co-authored by the National Renewable Energy Laboratory, operated by the Alliance for Sustainable Energy, LLC, for the U.S. Department of Energy (DOE) under Contract No. DE-AC36-08GO28308. The views expressed in the article do not necessarily represent the views of the DOE or the U.S. Government. The U.S. Government retains and the publisher, by accepting the article for publication, acknowledges that the U.S. Government retains a nonexclusive, paid-up, irrevocable, worldwide license to publish or reproduce the published form of this work, or allow others to do so, for U.S. Government purposes. Funding for the original work was provided by the U.S. Department of Energy Grid Modernization Laboratory Consortium. The authors thank Caitlin Murphy, Donald Jenket, Richard Garrett, Heather Scott, John Eddy, Christopher Sibrel, Logan Creelman, and Sam Alvord for their feedback and support. Finally, the authors thank two anonymous reviewers whose feedback improved the quality of the paper.

Appendix A. Model ($\mathcal{R}$) (REopt) formulation

This appendix introduces the complete formulation of the mixed-integer linear programming formulation used in our methodology. The formulation is a direct extension of both Hirwa et al. and Ogunmodede et al. [66,80]. We first provide notation used for these additions, in alphabetic order, and categorized as: (i) indices and sets, (ii) parameters, and (iii) variables. Our naming convention represents sets using calligraphic capital letters, parameters employing lower-case letters, and variables invoking upper-case letters. Subscripts denote indices, whereas superscripts and other "decorations" represent similar constructs such as scenarios with the same "stem". This formulation spans the equivalent of a single scenario-year pairing in our model ($\mathcal{P}$), for which we provide more details in Appendix B.

A.1. Sets and parameters

Sets	
$\mathcal{B}$	Storage systems
$\mathcal{C}$	Technology classes
$\mathcal{D}$	Time-of-use demand periods
$\mathcal{E}$	Electrical time-of-use demand tiers
$\mathcal{F}$	Fuel types
$\mathcal{H}$	Time steps
$\mathcal{K}$	Subdivisions of power rating
$\mathcal{M}$	Months of the year
$\mathcal{N}$	Monthly peak demand tiers
$\mathcal{O}$	Outages (groups of consecutive hours)
$\mathcal{S}$	Power rating segments
$\mathcal{T}$	Technologies
$\mathcal{U}$	Total electrical energy pricing tiers
$\mathcal{V}$	Net metering regimes
Subsets and indexed sets	
$\mathcal{B}^{\mathrm{e}} \subseteq \mathcal{B}$	Electrical storage systems
$\mathcal{B}^{\mathrm{c}} \subseteq \mathcal{B}^{\mathrm{th}}$	Cold thermal energy storage systems
$\mathcal{B}^{\mathrm{h}} \subseteq \mathcal{B}^{\mathrm{th}}$	Hot thermal energy storage systems
$\mathcal{B}^{\mathrm{th}} \subseteq \mathcal{B}$	Thermal energy storage systems
$\mathcal{F}^{\mathrm{d}} \subseteq \mathcal{F}$	Diesel fuel
$\mathcal{H}_d \subseteq \mathcal{H}$	Time steps within electrical power time-of-use demand tier d
$\mathcal{H}^{\mathrm{g}} \subseteq \mathcal{H}$	Time steps in which grid purchasing is available
$\mathcal{H}_m \subseteq \mathcal{H}$	Time steps within a given month m
$\mathcal{K}_t \subseteq \mathcal{K}$	Subdivisions applied to technology t
$\mathcal{K}^{\mathrm{c}} \subseteq \mathcal{K}$	Capital cost subdivisions
$\mathcal{M}^{\mathrm{lb}}$	Look-back months considered for peak pricing
$\mathcal{S}_{tk} \subseteq \mathcal{S}$	Power rating segments from subdivision k applied to technology t
$\mathcal{T}_b \subseteq \mathcal{T}$	Technologies that can charge storage system b
$\mathcal{T}_c \subseteq \mathcal{T}$	Technologies in class c
$\mathcal{T}_f \subseteq \mathcal{T}$	Technologies that burn fuel type f
$\mathcal{T}_u \subseteq \mathcal{T}$	Technologies that may access electrical energy sales pricing tier u
$\mathcal{T}_v \subseteq \mathcal{T}$	Technologies that may access net-metering regime v
$\mathcal{T}^{\mathrm{ac}} \subseteq \mathcal{T}^{\mathrm{cl}}$	Absorption chillers
$\mathcal{T}^{\mathrm{CHP}} \subseteq \mathcal{T}^{\mathrm{f}}$	CHP technologies
$\mathcal{T}^{\mathrm{cl}} \subseteq \mathcal{T}$	Cooling technologies
$\mathcal{T}^{\mathrm{e}} \subseteq \mathcal{T}$	Electricity-producing technologies
$\mathcal{T}^{\mathrm{ec}} \subseteq \mathcal{T}^{\mathrm{cl}}$	Electric chillers

$\mathcal{T}^{\mathrm{f}} \subseteq \mathcal{T}^{\mathrm{e}}$	Fuel-burning, electricity-producing technologies
$\mathcal{T}^{\mathrm{g}} \subseteq \mathcal{T}^{\mathrm{e}}$	Generator technologies
$\mathcal{T}^{\mathrm{ht}} \subseteq \mathcal{T}$	Heating technologies
$\mathcal{T}^{\mathrm{td}} \subseteq \mathcal{T}$	Technologies that cannot turn down, i.e., PV and wind
$\mathcal{U}^{\mathrm{c}} \subseteq \mathcal{U}^{\mathrm{s}}$	Electrical energy curtailment pricing tiers
$\mathcal{U}^{\mathrm{nm}} \subseteq \mathcal{U}^{s}$	Electrical energy sales pricing tiers used in net metering
$\mathcal{U}^{\mathrm{s}} \subseteq \mathcal{U}$	Electrical energy sales pricing tiers
$\mathcal{U}^{\mathrm{s}}_{t} \subseteq \mathcal{U}^{\mathrm{s}}$	Electrical energy sales pricing tiers accessible by technology t
$\mathcal{U}^{\mathrm{sb}} \subseteq \mathcal{U}^{\mathrm{s}}$	Electrical energy sales pricing tiers accessible by storage

Scaling parameters

M	Sufficiently large number	[various]
Δ	Time step scaling	[h]

Parameters for costs and their functional forms

c^{afc}	Utility annual fixed charge	[$]
c^{amc}	Utility annual minimum charge	[$]
c^{cb}_{ts}	y-intercept of capital cost curve for technology t in segment s	[$]
c^{cm}_{ts}	Slope of capital cost curve for technology t in segment s	[$/kW]
c^{e}_{uh}	Export rate for energy in energy demand tier u in time step h	[$/kWh]
c^{g}_{uh}	Grid energy cost in energy demand tier u during time step h	[$/kWh]
c^{kW}_{b}	Capital cost of power capacity for storage system b	[$/kW]
c^{kWh}_{b}	Capital cost of energy capacity for storage system b	[$/kWh]
c^{omb}_{b}	Operation and maintenance cost of storage system b per unit of energy rating	[$/kWh]
c^{omp}_{t}	Operation and maintenance cost of technology t per unit of production	[$/kWh]
$c^{\mathrm{om}\sigma}_{t}$	Operation and maintenance cost of technology t per unit of power rating, including standby charges	[$/kW]
c^{r}_{de}	Cost per unit peak demand in time-of-use demand period d and tier e	[$/kW]
c^{rm}_{mn}	Cost per unit peak demand in tier n during month m	[$/kW]
c^{u}_{f}	Unit cost of fuel type f	[$/MMBTU]
c^{uml}	Cost of unmet load	[$/kWh]

Demand parameters

δ^{d}_{h}	Electrical load in time step h	[kW]
δ^{c}_{h}	Cooling load in time step h	[kW]
$\bar{\delta}^{\mathrm{gs}}_{u}$	Maximum allowable sales in electrical energy demand tier u	[kWh]
δ^{h}_{h}	Heating load in time step h	[kW]
δ^{lp}	Look-back proportion for ratchet charges	[fraction]
$\bar{\delta}^{\mathrm{mt}}_{n}$	Maximum monthly electrical power demand in peak pricing tier n	[kW]
$\bar{\delta}^{\mathrm{t}}_{e}$	Maximum power demand in time-of-use demand tier e	[kW]
$\bar{\delta}^{\mathrm{tu}}_{u}$	Maximum monthly electrical energy demand in tier u	[kWh]

Incentive parameters

$\bar{\imath}_{t}$	Upper incentive limit for technology t	[$]
i^{n}_{v}	Net metering limits in net metering regime v	[kW]
i^{r}_{t}	Incentive rate for technology t	[$/kWh]
$\bar{\imath}^{\sigma}_{t}$	Maximum power rating for obtaining production incentive for technology t	[kW]

Technology-specific time-series factor parameters

f^{ed}_{th}	Electrical power derate factor of technology t at time step h	[unitless]
f^{fa}_{th}	Fuel burn ambient correction factor of technology t at time step h	[unitless]
f^{ha}_{th}	Hot water ambient correction factor of technology t at time step h	[unitless]
f^{ht}_{th}	Hot water thermal grade correction factor of technology t at time step h	[unitless]
f^{p}_{th}	Production factor of technology t during time step h	[unitless]

Technology-specific factor parameters

f^{d}_{t}	Derate factor for turbine technology t	[unitless]
f^{l}_{t}	Levelization factor of technology t	[fraction]
f^{li}_{t}	Levelization factor of production incentive for technology t	[fraction]
f^{pf}_{t}	Present worth factor for fuel for technology t	[unitless]
f^{pi}_{t}	Present worth factor for incentives for technology t	[unitless]
$\underline{f}^{\mathrm{td}}_{t}$	Minimum turn down for technology t	[unitless]

Generic factor parameters

f^{e}	Energy present worth factor	[unitless]
f^{om}	O&M present worth factor	[unitless]
f^{tot}	Tax rate factor for off-taker	[fraction]
f^{tow}	Tax rate factor for owner	[fraction]

Power rating and fuel limit parameters

b^{fa}_{f}	Amount of available fuel of type f	[MMBTU]
$\underline{b}^{\sigma}_{c}$	Minimum power rating for technology class c	[kW]
$\bar{b}^{\sigma}_{t}$	Maximum power rating for technology t	[kW]
$\underline{b}^{\sigma\mathrm{s}}_{tks}$	Minimum power rating for technology t, subdivision k, segment s	[kW]
$\bar{b}^{\sigma\mathrm{s}}_{tks}$	Maximum power rating for technology t, subdivision k, segment s	[kW]

Efficiency parameters

η^{+}_{bt}	Efficiency of charging storage system b using technology t	[fraction]
η^{-}_{b}	Efficiency of discharging storage system b	[fraction]
η^{ac}	Absorption chiller efficiency	[fraction]
η^{b}	Boiler efficiency	[fraction]
η^{ec}	Electric chiller efficiency	[fraction]
$\eta^{\mathrm{g}+}$	Efficiency of charging electrical storage using grid power	[fraction]

Storage parameters

$\bar{\upsilon}^{\mathrm{bkW}}_{b}$	Maximum power output of storage system b	[kW]
$\underline{\upsilon}^{\mathrm{bkW}}_{b}$	Minimum power output of storage system b	[kW]
$\bar{\upsilon}^{\mathrm{bkWh}}_{b}$	Maximum energy capacity of storage system b	[kWh]

$\underline{u}_b^{\text{bkWh}}$	Minimum energy capacity of storage system b	[kWh]
ω_b^{d}	Decay rate of storage system b	[1/h]
$\underline{u}_b^{\text{mcp}}$	Minimum percent state of charge of storage system b	[fraction]
ω_b^0	Initial percent state of charge of storage system b	[fraction]
Fuel burn parameters		
m_t^{fb}	y-intercept of the fuel rate curve for technology t	[MMBTU/h]
m_t^{fbm}	Fuel burn rate y-intercept per unit size for technology t	[MMBTU/kWh]
m_t^{fm}	Slope of the fuel rate curve for technology t	[MMBTU/kWh]
CHP thermal performance parameters		
k_t^{te}	Thermal energy production of CHP technology t per unit electrical output	[unitless]
k_t^{tp}	Thermal power production of CHP technology t per unit power rating	[unitless]

A.2. Variables

Boundary conditions		
$X_{b,0}^{\text{se}}$	Initial state of charge for storage system b	[kWh]
Continuous variables		
X_b^{bkW}	Power rating for storage system b	[kW]
X_b^{bkWh}	Energy rating for storage system b	[kWh]
X_{de}^{de}	Peak electrical power demand allocated to tier e and time-of-use demand period d	[kW]
X_{bh}^{dfs}	Power discharged from storage system b during time step h	[kW]
X_{mn}^{dn}	Peak electrical power demand allocated to tier n during month m	[kW]
X_{th}^{f}	Fuel burned by technology t in time step h	[MMBTU/h]
X_{th}^{fb}	y-intercept of fuel burned by technology t in time step h	[MMBTU/h]
X_{uh}^{g}	Power purchased from the grid for electrical load in demand tier u during time step h	[kW]
X_h^{gts}	Electrical power delivered to storage by the grid in time step h	[kW]
X^{mc}	Annual utility minimum charge adder	[$]
X_t^{pi}	Production incentive collected for technology t	[$]
X^{plb}	Peak electrical demand during look back periods	[kW]
X_{tuh}^{ptg}	Exports from production to the grid by technology t in demand tier u during time step h	[kW]
X_{bth}^{pts}	Power from technology t used to charge storage system b during time step h	[kW]
X_{th}^{ptw}	Thermal power from technology t sent to waste or curtailed during time step h	[kW]
X_{th}^{rp}	Rated production of technology t during time step h	[kW]
X_t^{σ}	Power rating of technology t	[kW]
$X_{tks}^{\sigma\text{s}}$	Power rating of technology t allocated to subdivision k, segment s	[kW]
X_{bh}^{se}	State of charge of storage system b at the end of time step h	[kW]
X_{uh}^{stg}	Exports from storage to the grid in demand tier u during time step h	[kW]
X_{th}^{tp}	Thermal production of technology t in time step h	[kW]
X_{th}^{tpb}	y-intercept of thermal production of CHP technology t in time step h	[kW]
X_h^{uml}	Unmet load at time step h	[kW]
Binary variables		
Z_{mn}^{dmt}	1 If tier n has allocated demand during month m; 0 otherwise	[unitless]
Z_{de}^{dt}	1 if tier e has allocated demand during time-of-use period d; 0 otherwise	[unitless]
Z_v^{nmil}	1 If generation is in net metering interconnect limit regime v; 0 otherwise	[unitless]
Z_t^{pi}	1 If production incentive is available for technology t; 0 otherwise	[unitless]
$Z_{tks}^{\sigma\text{s}}$	1 If technology t in subdivision k, segment s is chosen; 0 otherwise	[unitless]
Z_{th}^{to}	1 If technology t is operating in time step h; 0 otherwise	[unitless]
Z_{mu}^{ut}	1 If demand tier u is active in month m; 0 otherwise	[unitless]

A.3. Objective function

$$
\begin{aligned}
(\hat{\mathcal{R}}) \quad \text{minimize} \; & \underbrace{\sum_{t\in\mathcal{T},k\in\mathcal{K}^{\text{c}},s\in\mathcal{S}_{tk}} \left(c_{ts}^{\text{cm}} \cdot X_{tks}^{\sigma\text{s}} + c_{ts}^{\text{cb}} \cdot Z_{tks}^{\sigma\text{s}} \right)}_{\text{Generating Technology Capital Costs}} \\
& + \underbrace{\sum_{b\in\mathcal{B}} \left(c_b^{\text{kW}} \cdot X_b^{\text{bkW}} + (c_b^{\text{kWh}} + c_b^{\text{omb}}) \cdot X_b^{\text{bkWh}} \right)}_{\text{Storage Capital Costs}} + \\
& (1 - f^{\text{tow}}) \cdot f^{\text{om}} \cdot \left(\underbrace{\sum_{t\in\mathcal{T}} c_t^{\text{om}\sigma} \cdot X_t^{\sigma}}_{\text{Fixed O\&M Costs}} + \underbrace{\sum_{t\in\mathcal{T}^{\text{f}},h\in\mathcal{H}} c_t^{\text{omp}} \cdot X_{th}^{\text{rp}}}_{\text{Variable O\&M Costs}} \right) \\
& + (1 - f^{\text{tot}}) \cdot \underbrace{\Delta \cdot \sum_{f\in\mathcal{F}} c_f^{\text{u}} \cdot \sum_{t\in\mathcal{T}_f,h\in\mathcal{H}} f_t^{\text{pf}} \cdot X_{th}^{\text{f}}}_{\text{Fuel Charges}} + \\
& \underbrace{\sum_{h\in\mathcal{H}} X_h^{\text{uml}}}_{\text{Unmet Load Costs}} + (1 - f^{\text{tot}}) \cdot f^{\text{e}} \cdot \left(\underbrace{\Delta \cdot \sum_{u\in\mathcal{U}^{\text{p}},h\in\mathcal{H}^{\text{g}}} c_{uh}^{\text{g}} \cdot X_{uh}^{\text{g}}}_{\text{Grid Energy Charges}} \right. \\
& + \underbrace{\sum_{d\in\mathcal{D},e\in\mathcal{E}} c_{de}^{\text{r}} \cdot X_{de}^{\text{de}}}_{\text{Time-of-Use Demand Charges}} + \underbrace{\sum_{m\in\mathcal{M},n\in\mathcal{N}} c_{mn}^{\text{rm}} \cdot X_{mn}^{\text{dn}}}_{\text{Monthly Demand Charges}} + \\
& \underbrace{c^{\text{afc}} + X^{\text{mc}}}_{\text{Fixed Charges}} \left. \underbrace{- \Delta \cdot \left(\sum_{h\in\mathcal{H}^{\text{g}}} \left(\sum_{u\in\mathcal{U}^{\text{sb}}} c_{uh}^{\text{e}} \cdot X_{uh}^{\text{stg}} + \sum_{t\in\mathcal{T},u\in\mathcal{U}_t^{\text{s}}} c_{uh}^{\text{e}} \cdot X_{tuh}^{\text{ptg}} \right) \right)}_{\text{Energy Export Payment}} \right) \\
& - (1 - f^{\text{tow}}) \cdot \underbrace{\sum_{t\in\mathcal{T}} X_t^{\text{pi}}}_{\text{Production Incentives}}
\end{aligned}
$$

The objective function is the same as that in $(\mathcal{R})$ and minimizes energy life cycle cost, i.e., capital costs, O&M costs, and utility costs; it maximizes (by subtracting) payments for energy exports and other incentives.

A.4. Constraints

We mathematically present and describe the remaining constraints from [14].

A.4.1. Fuel constraints

$$\Delta \cdot \sum_{t \in \mathcal{T}_f, h \in \mathcal{H}} X^{\mathrm{f}}_{th} \leq b^{\mathrm{fa}}_{f} \quad \forall f \in \mathcal{F} \setminus \mathcal{F}^{\mathrm{d}} \tag{A.1a}$$

$$\Delta \cdot \sum_{t \in \mathcal{T}_f, h \in \mathcal{H}^{\mathrm{out}}_o} X^{\mathrm{f}}_{th} \leq b^{\mathrm{fa}}_{f} \quad \forall f \in \mathcal{F}^{\mathrm{d}}, o \in \mathcal{O} \tag{A.1b}$$

$$X^{\mathrm{f}}_{th} = m^{\mathrm{fm}}_{t} \cdot f^{\mathrm{p}}_{th} \cdot X^{\mathrm{rp}}_{th} + m^{\mathrm{fb}}_{t} \cdot Z^{\mathrm{to}}_{th} \quad \forall t \in \mathcal{T}^{\mathrm{g}}, h \in \mathcal{H} \tag{A.1c}$$

$$X^{\mathrm{f}}_{th} = f^{\mathrm{fa}}_{th} \cdot \left(X^{\mathrm{fb}}_{th} + f^{\mathrm{p}}_{th} \cdot m^{\mathrm{fm}}_{t} \cdot X^{\mathrm{rp}}_{th}\right) \quad \forall t \in \mathcal{T}^{CHP}, h \in \mathcal{H} \tag{A.1d}$$

$$m^{\mathrm{fbm}}_{t} \cdot X^{\sigma}_{t} - M \cdot (1 - Z^{\mathrm{to}}_{th}) \leq X^{\mathrm{fb}}_{th} \quad \forall t \in \mathcal{T}^{\mathrm{CHP}}, h \in \mathcal{H} \tag{A.1e}$$

$$X^{\mathrm{f}}_{th} = m^{\mathrm{fm}}_{t} \cdot X^{\mathrm{tp}}_{th} \quad \forall t \in \mathcal{T}^{\mathrm{ht}} \setminus \mathcal{T}^{CHP}, \ h \in \mathcal{H} \tag{A.1f}$$

Constraints (A.1a)–(A.1c) enforce the fuel requirements for the combustion-powered technologies. Specifically, constraint (A.1a) limits the available quantity for each fuel type except for diesel (e.g., natural gas) per annum. Constraint (A.1a) is consistent with [14] with the exception of the removal of the diesel generator technology, which is now treated separately in constraint (A.1b). Constraint (A.1b) limits the available quantity of diesel fuel consumed during an outage with the assumption that a tank gets refilled before the start of the next outage. Constraint (A.1c) calculates the amount of fuel burned by each diesel generator in each time step as a function of the generator's (i) power output and (ii) runtime, an assumption that [13] verify using industry fuel consumption data. Constraint (A.1d) defines fuel consumption for CHP systems using both a per-operating-hour rate and a per-unit-production rate; constraint (A.1e) sets this decision variable to a fixed proportion of the system's power rating if it is operating, and to zero otherwise. Constraint (A.1f) enforces a variable burn rate per unit of energy produced for each electric, non-CHP technology.

A.4.2. Thermal production constraints

$$X^{\mathrm{tpb}}_{th} \leq \min\left\{k^{\mathrm{tp}}_{t} \cdot X^{\sigma}_{t}, M \cdot Z^{\mathrm{to}}_{th}\right\} \quad \forall t \in \mathcal{T}^{\mathrm{CHP}}, h \in \mathcal{H} \tag{A.2a}$$

$$X^{\mathrm{tpb}}_{th} \geq k^{\mathrm{tp}}_{t} \cdot X^{\sigma}_{t} - M \cdot (1 - Z^{\mathrm{to}}_{th}) \quad \forall t \in \mathcal{T}^{\mathrm{CHP}}, h \in \mathcal{H} \tag{A.2b}$$

$$f^{\mathrm{ha}}_{th} \cdot f^{\mathrm{ht}}_{th} \cdot \left(k^{\mathrm{te}}_{t} \cdot f^{\mathrm{p}}_{th} \cdot X^{\mathrm{rp}}_{th} + X^{\mathrm{tpb}}_{th}\right) = X^{\mathrm{tp}}_{th} \quad \forall t \in \mathcal{T}^{\mathrm{CHP}}, h \in \mathcal{H} \tag{A.2c}$$

Constraints (A.2a)–(A.2b) limit the fixed component of thermal production of CHP technology t in time step h to the product of the thermal power production per unit of power rating and the power rating itself if the technology is operating, and 0 if it is not. Constraint (A.2c) relates the thermal production of a CHP technology to its constituent components, where the relationship includes a term that is proportional to electrical power production in each time step.

A.4.3. Storage system constraints

Boundary Conditions and Size Limits

$$X^{\mathrm{se}}_{b,0} = w^{0}_{b} \cdot X^{\mathrm{bkWh}}_{b} \quad \forall b \in \mathcal{B} \tag{A.3a}$$

$$\underline{w}^{\mathrm{bkWh}}_{b} \leq X^{\mathrm{bkWh}}_{b} \leq \bar{w}^{\mathrm{bkWh}}_{b} \quad \forall b \in \mathcal{B} \tag{A.3b}$$

$$\underline{w}^{\mathrm{bkW}}_{b} \leq X^{\mathrm{bkW}}_{b} \leq \bar{w}^{\mathrm{bkW}}_{b} \quad \forall b \in \mathcal{B} \tag{A.3c}$$

Constraint (A.3a) initializes a storage system's state of charge using a fraction of its energy rating; constraints (A.3b) and (A.3c) limit the storage system size under the implicit assumption that a storage system's power and energy ratings are independent. These constraints are identical to those given in ($\mathcal{R}$), but work in conjunction with significantly modified storage constraints that directly follow.

Storage Operations

$$X^{\mathrm{pts}}_{bth} + \sum_{u \in U^{\mathrm{s}}_{t}} X^{\mathrm{ptg}}_{tuh} \leq f^{\mathrm{p}}_{th} \cdot f^{\mathrm{l}}_{t} \cdot X^{\mathrm{rp}}_{th} \quad \forall b \in \mathcal{B}^{\mathrm{e}}, \ t \in \mathcal{T}^{\mathrm{e}}, \ h \in \mathcal{H}^{\mathrm{g}} \tag{A.3d}$$

$$X^{\mathrm{pts}}_{bth} \leq f^{\mathrm{p}}_{th} \cdot f^{\mathrm{l}}_{t} \cdot X^{\mathrm{rp}}_{th} \quad \forall b \in \mathcal{B}^{\mathrm{e}}, \ t \in \mathcal{T}^{\mathrm{e}}, \ h \in \mathcal{H} \setminus \mathcal{H}^{\mathrm{g}} \tag{A.3e}$$

$$X^{\mathrm{pts}}_{bth} \leq f^{\mathrm{p}}_{th} \cdot X^{\mathrm{tp}}_{th} \quad \forall b \in \mathcal{B}^{\mathrm{th}}, \ t \in \mathcal{T}_{b} \setminus \mathcal{T}^{\mathrm{CHP}}, \ h \in \mathcal{H} \tag{A.3f}$$

$$X^{\mathrm{pts}}_{bth} + X^{\mathrm{ptw}}_{th} \leq X^{\mathrm{tp}}_{th} \quad \forall b \in \mathcal{B}^{\mathrm{h}}, \ t \in \mathcal{T}^{\mathrm{CHP}}, \ h \in \mathcal{H} \tag{A.3g}$$

$$X^{\mathrm{se}}_{bh} = X^{\mathrm{se}}_{b,h-1} + \Delta \cdot \left(\sum_{t \in \mathcal{T}^{\mathrm{e}}} (\eta^{+}_{bt} \cdot X^{\mathrm{pts}}_{bth}) + \eta^{\mathrm{g}+} \cdot X^{\mathrm{gts}}_{h} - X^{\mathrm{dfs}}_{bh} / \eta^{-}_{b}\right)$$
$$\forall b \in \mathcal{B}^{\mathrm{e}}, \ h \in \mathcal{H}^{\mathrm{g}} \tag{A.3h}$$

$$X^{\mathrm{se}}_{bh} = X^{\mathrm{se}}_{b,h-1} + \Delta \cdot \left(\sum_{t \in \mathcal{T}^{\mathrm{e}}} (\eta^{+}_{bt} \cdot X^{\mathrm{pts}}_{bth}) - X^{\mathrm{dfs}}_{bh} / \eta^{-}_{b}\right)$$
$$\forall b \in \mathcal{B}^{\mathrm{e}}, \ h \in \mathcal{H} \setminus \mathcal{H}^{\mathrm{g}} \tag{A.3i}$$

$$X^{\mathrm{se}}_{bh} = X^{\mathrm{se}}_{b,h-1} + \Delta \cdot \left(\sum_{t \in \mathcal{T}_{b}} \eta^{+}_{bt} \cdot X^{\mathrm{pts}}_{bth} - X^{\mathrm{dfs}}_{bh} / \eta^{-}_{b} - w^{\mathrm{d}}_{b} \cdot X^{\mathrm{se}}_{bh}\right)$$
$$\forall b \in \mathcal{B}^{\mathrm{th}}, h \in \mathcal{H} \tag{A.3j}$$

$$X^{\mathrm{se}}_{bh} \geq \underline{w}^{\mathrm{mcp}}_{b} \cdot X^{\mathrm{bkWh}}_{b} \quad \forall b \in \mathcal{B}, h \in \mathcal{H} \tag{A.3k}$$

Constraints (A.3d) and (A.3e) restrict the electrical power that charges storage and is exported to the grid (in the former case), or that charges storage only (in the latter case, when grid export is unavailable) from each technology in each time step relative to the amount of electricity produced. Constraint (A.3f) provides an analogous restriction to that of constraint (A.3e) for thermal production, and constraint (A.3g) provides the same restriction for the thermal production of CHP systems. Constraints (A.3h), (A.3i), and (A.3j) balance state of charge for each storage system and time period for three specific cases, respectively: (i) available grid-purchased electricity, (ii) lack of grid-purchased electricity, and (iii) thermal storage, in which we account for decay. Constraint (A.3k) ensures that minimum state-of-charge requirements are not violated.

Charging Rates

$$X^{\mathrm{bkW}}_{b} \geq \sum_{t \in \mathcal{T}_{b}} X^{\mathrm{pts}}_{bth} + X^{\mathrm{gts}}_{h} + X^{\mathrm{dfs}}_{bh} \quad \forall b \in \mathcal{B}^{\mathrm{e}}, h \in \mathcal{H}^{\mathrm{g}} \tag{A.3l}$$

$$X^{\mathrm{bkW}}_{b} \geq \sum_{t \in \mathcal{T}_{b}} X^{\mathrm{pts}}_{bth} + X^{\mathrm{dfs}}_{bh} \quad \forall b \in \mathcal{B}^{\mathrm{e}}, h \in \mathcal{H} \setminus \mathcal{H}^{\mathrm{g}} \tag{A.3m}$$

$$X^{\mathrm{bkW}}_{b} \geq \sum_{t \in \mathcal{T}_{b}} X^{\mathrm{pts}}_{bth} + X^{\mathrm{dfs}}_{bh} \quad \forall b \in \mathcal{B}^{\mathrm{th}}, h \in \mathcal{H} \tag{A.3n}$$

$$X^{\mathrm{se}}_{bh} \leq X^{\mathrm{bkWh}}_{b} \quad \forall b \in \mathcal{B}, h \in \mathcal{H} \tag{A.3o}$$

Constraints (A.3l) and (A.3m) require that a battery's power rating must meet or exceed its rate of charge or discharge; the latter constraint considers the case in which the grid is not available. Constraint (A.3n) reflects the power requirements for the thermal system. Constraint (A.3o) requires a storage system's energy level to be at or below the corresponding rating.

Cold and hot thermal loads

$$\sum_{t \in \mathcal{T}^{cl}} f^{\mathrm{p}}_{th} \cdot X^{\mathrm{tp}}_{th} + \sum_{b \in \mathcal{B}^{\mathrm{c}}} X^{\mathrm{dfs}}_{bh} = \delta^{\mathrm{c}}_{h} \cdot \eta^{\mathrm{ec}} + \sum_{b \in \mathcal{B}^{\mathrm{c}}, t \in \mathcal{T}^{\mathrm{cl}}} X^{\mathrm{pts}}_{bth} \quad \forall h \in \mathcal{H} \tag{A.4a}$$

$$\sum_{t \in \mathcal{T}^{\mathrm{CHP}}} X^{\mathrm{tp}}_{th} + \sum_{t \in \mathcal{T}^{\mathrm{ht}} \setminus \mathcal{T}^{\mathrm{CHP}}} f^{\mathrm{p}}_{th} \cdot X^{\mathrm{tp}}_{th} + \sum_{b \in \mathcal{B}^{\mathrm{h}}} X^{\mathrm{dfs}}_{bh} = \delta^{\mathrm{h}}_{h} \cdot \eta^{\mathrm{b}} + \sum_{t \in \mathcal{T}^{\mathrm{CHP}}} X^{\mathrm{ptw}}_{th} + \sum_{b \in \mathcal{B}^{\mathrm{h}}, t \in \mathcal{T}^{\mathrm{ht}}} X^{\mathrm{pts}}_{bth} + \sum_{t \in \mathcal{T}^{\mathrm{ac}}} X^{\mathrm{tp}}_{th} / \eta^{\mathrm{ac}} \quad \forall h \in \mathcal{H} \tag{A.4b}$$

Constraints (A.4a) and (A.4b) balance cold and hot thermal loads, respectively, by equating the power production and the power from storage with the sum of the demand, the power to storage, and, in

the case of cold loads, from the absorption chillers as well. Here, for legacy reasons, we have scaled the power by the efficiency of the respective technology; based on our variable definitions, we could have equivalently adjusted these by a coefficient of performance.

A.4.4. Production constraints

$$X^{\mathrm{rp}}_{th} \le \bar{b}^{\sigma}_{t} \cdot Z^{\mathrm{to}}_{th} \quad \forall t \in \mathcal{T}, h \in \mathcal{H} \tag{A.5a}$$

$$\underline{f}^{\mathrm{td}}_{t} \cdot X^{\sigma}_{t} - X^{\mathrm{rp}}_{th} \le \bar{b}^{\sigma}_{t} \cdot (1 - Z^{\mathrm{to}}_{th}) \quad \forall t \in \mathcal{T}, h \in \mathcal{H} \tag{A.5b}$$

$$X^{\mathrm{tp}}_{th} \le X^{\sigma}_{t} \quad \forall t \in \mathcal{T} \setminus \mathcal{T}^{\mathrm{e}}, h \in \mathcal{H} \tag{A.5c}$$

Constraint set (A.5) ensures that the rated production lies between a minimum turn-down threshold and a maximum system size; constraints (A.5a) and (A.5b) are copied from [80], while constraint (A.5c) is new. Constraint (A.5a) restricts system power output to its rated capacity when the technology is operating, and to 0 otherwise. Constraint (A.5b) ensures a minimum power output while a technology is operating; otherwise, the constraint is dominated by simple bounds on production. Constraint (A.5c) ensures that the thermal production of non-CHP heating and cooling technologies does not exceed system size.

A.4.5. Production incentives

$$X^{\mathrm{pi}}_{t} \le \min\left\{ \bar{\imath}_{t} \cdot Z^{\mathrm{pi}}_{t}, \sum_{h \in \mathcal{H}} \Delta \cdot i^{\mathrm{r}}_{t} \cdot f^{\mathrm{pi}}_{t} \cdot f^{\mathrm{p}}_{th} \cdot f^{\mathrm{li}}_{t} \cdot X^{\mathrm{rp}}_{th} \right\} \quad \forall t \in \mathcal{T} \tag{A.6a}$$

$$X^{\sigma}_{t} \le \bar{\imath}^{\sigma}_{t} + \mathrm{M} \cdot (1 - Z^{\mathrm{pi}}_{t}) \quad \forall t \in \mathcal{T} \tag{A.6b}$$

Constraint (A.6a) calculates total production incentives, if available, for each technology. Constraint (A.6b) sets an upper bound on the size of system that qualifies for production incentives, if production incentives are available.

A.4.6. Power rating

$$X^{\sigma}_{t} \le \bar{b}^{\sigma}_{t} \cdot \sum_{s \in S_{tk}} Z^{\sigma s}_{tks} \quad \forall c \in C, t \in \mathcal{T}_{c}, k \in \mathcal{K}_{t} \tag{A.7a}$$

$$\sum_{t \in \mathcal{T}_{c}, s \in S_{tk}} Z^{\sigma s}_{tks} \le 1 \quad \forall c \in C, k \in \mathcal{K} \tag{A.7b}$$

$$\sum_{t \in \mathcal{T}_{c}} X^{\sigma}_{t} \ge \underline{b}^{\sigma}_{c} \quad \forall c \in C \tag{A.7c}$$

$$X^{\mathrm{rp}}_{th} = X^{\sigma}_{t} \quad \forall t \in \mathcal{T}^{\mathrm{td}}, h \in \mathcal{H} \tag{A.7d}$$

$$X^{\mathrm{rp}}_{th} \le f^{\mathrm{ed}}_{th} \cdot X^{\sigma}_{t} \quad \forall t \in \mathcal{T} \setminus \mathcal{T}^{\mathrm{td}}, h \in \mathcal{H} \tag{A.7e}$$

$$\underline{b}^{\sigma s}_{tks} \cdot Z^{\sigma s}_{tks} \le X^{\sigma s}_{tks} \le \bar{b}^{\sigma s}_{tks} \cdot Z^{\sigma s}_{tks} \quad \forall t \in \mathcal{T}, k \in \mathcal{K}_{t}, s \in S_{tk} \tag{A.7f}$$

$$\sum_{s \in S_{tk}} X^{\sigma s}_{tks} = X^{\sigma}_{t} \quad \forall t \in \mathcal{T}, k \in \mathcal{K}_{t} \tag{A.7g}$$

Constraint (A.7a) permits nonzero power ratings only for the selected technology and corresponding subdivision in each class. Constraint (A.7b) allows at most one technology to be chosen for each subdivision in each class. Constraint (A.7c) limits the power rating to the minimum allowed for a technology class. Constraint (A.7d) prevents renewable technologies from turning down; rather, they must provide output at their nameplate capacity. Constraint (A.7e) limits rated production from all non-renewable technologies to be less than or equal to the product of the power rating and the derate factor for each time period. Constraint (A.7f) imposes both lower and upper limits on power rating of a technology, allocated to a subdivision in a segment, and constraint (A.7g) sums the segment sizes to the total for a given technology and subdivision.

A.4.7. Load balancing and grid sales

$$\sum_{t \in \mathcal{T}^{\mathrm{e}} \setminus \mathcal{T}^{\mathrm{g}}} (f^{\mathrm{p}}_{th} \cdot f^{\mathrm{l}}_{t} \cdot X^{\mathrm{rp}}_{th}) + \sum_{b \in \mathcal{B}^{\mathrm{e}}} X^{\mathrm{dfs}}_{bh} + \sum_{u \in \mathcal{U}^{\mathrm{p}}} X^{\mathrm{g}}_{uh} = \sum_{t \in \mathcal{T}^{\mathrm{e}} \setminus \mathcal{T}^{\mathrm{g}}} \sum_{b \in \mathcal{B}^{\mathrm{e}}} X^{\mathrm{pts}}_{bth} + \sum_{t \in \mathcal{T}^{\mathrm{e}} \setminus \mathcal{T}^{\mathrm{g}}} \sum_{u \in \mathcal{U}^{\mathrm{s}}_{t}} X^{\mathrm{ptg}}_{tuh} + \sum_{u \in \mathcal{U}^{\mathrm{sb}}} X^{\mathrm{stg}}_{uh} + X^{\mathrm{gts}}_{h} + \sum_{t \in \mathcal{T}^{ec}} X^{\mathrm{tp}}_{th} / \eta^{\mathrm{ec}} + \delta^{\mathrm{d}}_{h} \quad \forall h \in \mathcal{H}^{g} \tag{A.8a}$$

$$\sum_{t \in \mathcal{T}^{\mathrm{e}}} (f^{\mathrm{p}}_{th} \cdot f^{\mathrm{l}}_{t} \cdot X^{\mathrm{rp}}_{th}) + \sum_{b \in \mathcal{B}^{\mathrm{e}}} X^{\mathrm{dfs}}_{bh} = \sum_{b \in \mathcal{B}^{\mathrm{e}}, t \in \mathcal{T}^{\mathrm{e}}} \left(X^{\mathrm{pts}}_{bth} + \sum_{u \in \mathcal{U}^{\mathrm{c}}} X^{\mathrm{ptg}}_{tuh} \right) + \sum_{t \in \mathcal{T}^{\mathrm{ec}}} X^{\mathrm{tp}}_{th} / \eta^{\mathrm{ec}} + \delta^{\mathrm{d}}_{h} \quad \forall h \in \mathcal{H} \setminus \mathcal{H}^{g} \tag{A.8b}$$

$$\sum_{u \in \mathcal{U}^{\mathrm{p}}} X^{\mathrm{g}}_{uh} \ge X^{\mathrm{gts}}_{h} \quad \forall h \in \mathcal{H}^{g} \tag{A.8c}$$

$$\sum_{b \in \mathcal{B}^{\mathrm{e}}} X^{\mathrm{dfs}}_{bh} \ge \sum_{u \in \mathcal{U}^{\mathrm{sb}}} X^{\mathrm{stg}}_{uh} \quad \forall h \in \mathcal{H}^{g} \tag{A.8d}$$

$$\Delta \cdot \sum_{h \in \mathcal{H}^{\mathrm{g}}} \left(X^{\mathrm{stg}}_{uh} + \sum_{t \in \mathcal{T}_{u}} X^{\mathrm{ptg}}_{tuh} \right) \le \bar{\delta}^{\mathrm{gs}}_{u} \quad \forall u \in \mathcal{U}^{\mathrm{sb}} \cap \mathcal{U}^{\mathrm{nm}} \tag{A.8e}$$

$$\Delta \cdot \sum_{h \in \mathcal{H}^{\mathrm{g}}, t \in \mathcal{T}_{u}} X^{\mathrm{ptg}}_{tuh} \le \bar{\delta}^{\mathrm{gs}}_{u} \quad \forall u \in \mathcal{U}^{\mathrm{nm}} \setminus \mathcal{U}^{\mathrm{sb}} \tag{A.8f}$$

$$X^{\mathrm{uml}}_{h} = \delta^{\mathrm{d}}_{h} - \sum_{t \in \mathcal{T}} f^{p}_{th} \cdot f^{l}_{t} \cdot X^{rp}_{th} - \sum_{b \in \mathcal{B}^{e}} X^{dfs}_{bh} - \sum_{u \in \mathcal{U}^{p}} X^{g}_{uh} + \sum_{t \in \mathcal{T}^{e} / \mathcal{T}^{g}} \sum_{b \in \mathcal{B}^{e}} X^{pts}_{bth} + \sum_{t \in \mathcal{T}^{e} / \mathcal{T}^{g}} \sum_{u \in \mathcal{U}^{s}_{t}} X^{ptg}_{tuh} + \sum_{u \in \mathcal{U}^{sb}} X^{stg}_{uh} \quad \forall\, h \in \mathcal{H},\ \omega \in \Omega \tag{A.8g}$$

Constraint (A.8a) balances load by requiring that the sum of power (i) produced, (ii) discharged from storage, and (iii) purchased from the grid is equal to the sum of (i) the power charged to storage, (ii) the power sold to the grid from in-house production or storage, (iii) the power charged to storage directly from the grid, (iv) any additional power consumed by the electric chiller (where this is an additional term relative to the original model ($\mathcal{R}$)), and (v) the electrical load on site. Constraint (A.8b) provides an analogous load-balancing requirement for hours in which the site is disconnected from the grid due to an outage (and contains the same additional term relative to the original model ($\mathcal{R}$)). Constraint (A.8c) restricts charging of storage from grid production to the grid power purchased for each hour. Similarly, constraint (A.8d) restricts the sales from the electrical storage system to its rate of discharge in each time period. Constraints (A.8e) and (A.8f) restrict the annual energy sold to the grid at net-metering rates; only one of these is implemented in each case according to user-specified options. While a collection of pre-specified technologies may contribute to net-metering rates in both cases, constraint (A.8e) allows storage to contribute to net-metering while constraint (A.8f) does not.

A.4.8. Rate tariff constraints

Net Metering

$$\sum_{v \in \mathcal{V}} Z^{\mathrm{nmil}}_{v} = 1 \tag{A.9a}$$

$$\sum_{t \in \mathcal{T}_{v}} f^{\mathrm{d}}_{t} \cdot X^{\sigma}_{t} \le i^{\mathrm{n}}_{v} \cdot Z^{\mathrm{nmil}}_{v} \quad \forall v \in \mathcal{V} \tag{A.9b}$$

$$\Delta \cdot \sum_{h \in \mathcal{H}^{\mathrm{g}}} \left(\sum_{u \in \mathcal{U}^{\mathrm{nm}}, t \in \mathcal{T}_{u}} X^{\mathrm{ptg}}_{tuh} + \sum_{u \in \mathcal{U}^{\mathrm{nm}} \cap \mathcal{U}^{\mathrm{sb}}} X^{\mathrm{stg}}_{uh} \right) \le \Delta \cdot \sum_{u \in \mathcal{U}^{\mathrm{p}}, h \in \mathcal{H}^{\mathrm{g}}} X^{\mathrm{g}}_{uh} \tag{A.9c}$$

Constraint (A.9a) limits the net metering to a single regime at a time. Constraint (A.9b) restricts the sum of the power rating of all technologies to be less than or equal to the net metering regime.

Constraint (A.9c) ensures that energy sales at net-metering rates do not exceed the energy purchased from the grid.

Monthly Total Demand Charges

$$\Delta \cdot \sum_{h \in \mathcal{H}_m} X^{\mathrm{g}}_{uh} \leq \bar{\delta}^{\mathrm{tu}}_{u} \cdot Z^{\mathrm{ut}}_{mu} \quad \forall m \in \mathcal{M}, u \in \mathcal{U}^{\mathrm{p}} \tag{A.10a}$$

$$Z^{\mathrm{ut}}_{mu} \leq Z^{\mathrm{ut}}_{m,u-1} \quad \forall u \in \mathcal{U}^{\mathrm{p}} : u \geq 2, m \in \mathcal{M} \tag{A.10b}$$

$$\bar{\delta}^{\mathrm{tu}}_{u-1} \cdot Z^{\mathrm{ut}}_{mu} \leq \Delta \cdot \sum_{h \in \mathcal{H}_m} X^{\mathrm{g}}_{u-1,h} \quad \forall u \in \mathcal{U}^{\mathrm{p}} : u \geq 2, m \in \mathcal{M} \tag{A.10c}$$

Constraint (A.10a) limits the quantity of electrical energy purchased from the grid in a given month from a specified pricing tier to the maximum available. Constraint (A.10b) forces pricing tiers to be charged in a specific order, and constraint (A.10c) forces one pricing tier's purchases to be at capacity if any charges are applied to the next tier.

Peak Power Demand Charges: Months

$$X^{\mathrm{dn}}_{mn} \leq \bar{\delta}^{\mathrm{mt}}_{n} \cdot Z^{\mathrm{dmt}}_{mn} \quad \forall n \in \mathcal{N}, m \in \mathcal{M} \tag{A.11a}$$

$$Z^{\mathrm{dmt}}_{mn} \leq Z^{\mathrm{dmt}}_{m,n-1} \quad \forall n \in \mathcal{N} : n \geq 2, m \in \mathcal{M} \tag{A.11b}$$

$$\bar{\delta}^{\mathrm{mt}}_{n-1} \cdot Z^{\mathrm{dmt}}_{mn} \leq X^{\mathrm{dn}}_{m,n-1} \quad \forall n \in \mathcal{N} : n \geq 2, m \in \mathcal{M} \tag{A.11c}$$

$$\sum_{n \in \mathcal{N}} X^{\mathrm{dn}}_{mn} \geq \sum_{u \in \mathcal{U}^{\mathrm{p}}} X^{\mathrm{g}}_{uh} \quad \forall m \in \mathcal{M}, h \in \mathcal{H}_m \tag{A.11d}$$

Constraint (A.11a) limits the energy demand allocated to each tier to no more than the maximum demand allowed. Constraint (A.11b) forces monthly demand tiers to become active in a prespecified order. Constraint (A.11c) forces demand to be met in one tier before the next demand tier. Constraint (A.11d) defines the peak demand to be greater than or equal to all of the demands across the time horizon, where an equality is actually induced by the sense of the objective function. A user-defined option precludes CHP technology production from reducing peak demand; if selected, constraint (A.11d) becomes:

$$\sum_{n \in \mathcal{N}} X^{\mathrm{dn}}_{mn} \geq \sum_{u \in \mathcal{U}^{\mathrm{p}}} X^{\mathrm{g}}_{uh} + \sum_{t \in \mathcal{T}^{\mathrm{CHP}}} \left(f^{\mathrm{p}}_{th} \cdot f^{\mathrm{l}}_{t} \cdot X^{\mathrm{rp}}_{th} - \sum_{b \in \mathcal{B}^{\mathrm{h}}} X^{\mathrm{pts}}_{bth} - \sum_{u \in \mathcal{U}^{s}_{t}} X^{\mathrm{ptg}}_{tuh} \right)$$
$$\forall m \in \mathcal{M}, h \in \mathcal{H}_m.$$

Peak Power Demand Charges: Time-of-Use Demand and Ratchet Charges

$$X^{\mathrm{de}}_{de} \leq \bar{\delta}^{\mathrm{t}}_{e} \cdot Z^{\mathrm{dt}}_{de} \quad \forall e \in \mathcal{E}, d \in \mathcal{D} \tag{A.12a}$$

$$Z^{\mathrm{dt}}_{de} \leq Z^{\mathrm{dt}}_{d,e-1} \quad \forall e \in \mathcal{E} : e \geq 2, d \in \mathcal{D} \tag{A.12b}$$

$$\bar{\delta}^{\mathrm{t}}_{e-1} \cdot Z^{\mathrm{dt}}_{de} \leq X^{\mathrm{de}}_{d,e-1} \quad \forall e \in \mathcal{E} : e \geq 2, d \in \mathcal{D} \tag{A.12c}$$

$$\sum_{e \in \mathcal{E}} X^{\mathrm{de}}_{de} \geq \max \left\{ \sum_{u \in \mathcal{U}^{\mathrm{p}}} X^{\mathrm{g}}_{uh}, \delta^{\mathrm{lp}} \cdot X^{\mathrm{plb}} \right\} \quad \forall d \in \mathcal{D}, h \in \mathcal{H}_d \tag{A.12d}$$

$$X^{\mathrm{plb}} \geq \sum_{n \in \mathcal{N}} X^{\mathrm{dn}}_{mn} \quad \forall m \in \mathcal{M}^{\mathrm{lb}} \tag{A.12e}$$

Constraints (A.12a)–(A.12d) correspond to constraints (A.11a)–(A.11d), respectively, but pertain to a type of charge not related to monthly use, but rather to time of use within a month. These *ratchet charges* are implemented using constraints (A.12d). The charge applied for each time-of-use period is a linearizable function of the greater of the peak electrical demand during that period (as given by the first term on the right-hand side of (A.12d)) and a fraction of the peak demand that occurs over a collection of months (known as *look-back months*) during the year (as given by the second term on the right-hand side of (A.12d)). Constraint (A.12e) ensures the peak demand over the set of look-back months is no lower than the peak demand for each look-back month. In this way, charges are based not only on use in a given month, but also on a fraction of use over the last several months, and becomes relevant when this latter use is high relative to current use. If CHP technologies are not allowed to reduce peak demand, constraint (A.12d) becomes:

$$\sum_{e \in \mathcal{E}} X^{\mathrm{de}}_{de} \geq \sum_{u \in \mathcal{U}^{\mathrm{p}}} X^{\mathrm{g}}_{uh} + \sum_{t \in \mathcal{T}^{\mathrm{CHP}}} \left(f^{\mathrm{p}}_{th} \cdot f^{\mathrm{l}}_{t} \cdot X^{\mathrm{rp}}_{th} - \sum_{b \in \mathcal{B}^{\mathrm{h}}} X^{\mathrm{pts}}_{bth} - \sum_{u \in \mathcal{U}^{s}_{t}} X^{\mathrm{ptg}}_{tuh} \right)$$
$$\forall d \in \mathcal{D}, h \in \mathcal{H}_d$$

A.4.9. Minimum utility charge

$$X^{\mathrm{mc}} \geq c^{\mathrm{amc}} - \underbrace{\left(\Delta \cdot \sum_{u \in \mathcal{U}^{\mathrm{p}}, h \in \mathcal{H}^{\mathrm{g}}} c^{\mathrm{g}}_{uh} \cdot X^{\mathrm{g}}_{uh} \right.}_{\text{Grid Energy Charges}} + \underbrace{\sum_{d \in \mathcal{D}, e \in \mathcal{E}} c^{\mathrm{r}}_{de} \cdot X^{\mathrm{de}}_{de}}_{\text{Time-of-Use Demand Charges}}$$
$$+ \underbrace{\sum_{m \in \mathcal{M}, n \in \mathcal{N}} c^{\mathrm{rm}}_{mn} \cdot X^{\mathrm{dn}}_{mn}}_{\text{Monthly Demand Charges}} -$$
$$\underbrace{\left. \Delta \cdot \left(\sum_{h \in \mathcal{H}^{\mathrm{g}}} \left(\sum_{u \in \mathcal{U}^{\mathrm{sb}}} c^{\mathrm{e}}_{uh} \cdot X^{\mathrm{stg}}_{uh} + \sum_{t \in \mathcal{T}, u \in \mathcal{U}^{s}_{t}} c^{\mathrm{e}}_{uh} \cdot X^{\mathrm{ptg}}_{tuh} \right) \right) \right)}_{\text{Energy Export Payment}} \tag{A.13}$$

Constraint (A.13) enforces a minimum payment to the utility provider, which is a fixed constant less charges incurred from grid energy, time-of-use demand and monthly demand payments, plus sales from exports to the grid.

A.4.10. Non-negativity

$$X^{\mathrm{plb}}, X^{\mathrm{mc}} \geq 0 \tag{A.14a}$$

$$X^{\sigma}_{t}, X^{\mathrm{pi}}_{t} \geq 0 \quad \forall t \in \mathcal{T} \tag{A.14b}$$

$$X^{\mathrm{ptg}}_{tuh} \geq 0 \quad \forall u \in \mathcal{U}, t \in \mathcal{T}_u, h \in \mathcal{H} \tag{A.14c}$$

$$X^{\mathrm{stg}}_{uh}, X^{\mathrm{g}}_{uh} \geq 0 \quad \forall u \in \mathcal{U}, h \in \mathcal{H} \tag{A.14d}$$

$$X^{\mathrm{de}}_{de} \geq 0 \quad \forall d \in \mathcal{D}, e \in \mathcal{E} \tag{A.14e}$$

$$X^{\mathrm{dn}}_{mn} \geq 0 \quad \forall m \in \mathcal{M}, n \in \mathcal{N} \tag{A.14f}$$

$$X^{\mathrm{gts}}_{h}, X^{\mathrm{uml}}_{h} \geq 0 \quad h \in \mathcal{H} \tag{A.14g}$$

$$X^{\mathrm{bkW}}_{b}, X^{\mathrm{bkWh}}_{b} \geq 0 \quad b \in \mathcal{B} \tag{A.14h}$$

$$X^{\sigma s}_{tks} \geq 0 \quad \forall t \in \mathcal{T}, k \in \mathcal{K}, s \in \mathcal{S}_{tk} \tag{A.14i}$$

$$X^{\mathrm{pts}}_{bth} \geq 0 \quad \forall b \in \mathcal{B}, t \in \mathcal{T}, h \in \mathcal{H} \tag{A.14j}$$

$$X^{\mathrm{se}}_{bh}, X^{\mathrm{dfs}}_{bh} \geq 0 \quad \forall b \in \mathcal{B}, h \in \mathcal{H} \tag{A.14k}$$

$$X^{\mathrm{rp}}_{th}, X^{\mathrm{f}}_{th}, X^{\mathrm{fb}}_{th}, X^{\mathrm{tpb}}_{th}, X^{\mathrm{tp}}_{th}, X^{\mathrm{ptw}}_{th} \geq 0 \quad \forall t \in \mathcal{T}, h \in \mathcal{H} \tag{A.14l}$$

A.4.11. Integrality

$$Z^{\mathrm{nmil}}_{v} \in \{0,1\} \quad \forall v \in \mathcal{V} \tag{A.15a}$$

$$Z^{\sigma s}_{tks} \in \{0,1\} \quad \forall t \in \mathcal{T}, k \in \mathcal{K}, s \in \mathcal{S}_{tk} \tag{A.15b}$$

$$Z^{\mathrm{pi}}_{t} \in \{0,1\} \quad \forall t \in \mathcal{T} \tag{A.15c}$$

$$Z^{\mathrm{to}}_{th} \in \{0,1\} \quad \forall t \in \mathcal{T}, h \in \mathcal{H} \tag{A.15d}$$

$$Z^{\mathrm{dt}}_{de} \in \{0,1\} \quad \forall d \in \mathcal{D}, e \in \mathcal{E} \tag{A.15e}$$

$$Z^{\mathrm{dmt}}_{mn} \in \{0,1\} \quad \forall m \in \mathcal{M}, n \in \mathcal{N} \tag{A.15f}$$

$$Z^{\mathrm{ut}}_{mu} \in \{0,1\} \quad \forall m \in \mathcal{M}, u \in \mathcal{U} \tag{A.15g}$$

Finally, constraints (A.14) ensure all of the variables in our formulation assume non-negative values. In addition to non-negativity restrictions, constraints (A.15) establish the integrality of the appropriate variables.

Appendix B. Mapping ($\mathcal{P}$) to ($\mathcal{R}$)

A single-scenario instance of model ($\mathcal{P}$) (i.e., $|\Omega| = 1$) is a condensed version of the formulation of REopt, ($\mathcal{R}$), detailed above in Appendix A. The variables in ($\mathcal{P}$) are indexed by scenario-year pairing, ω. Therefore, for a specific scenario-year pair (i.e., with ω fixed), we can present a complete mapping of our formulation to the expanded version. Every decision variable and constraint in ($\mathcal{R}$) can be mapped to a variable and constraint in a scenario-year-specific instance of ($\mathcal{P}$), respectively.

The technology and system sizing variable X from $\mathcal{P}$ is mapped to the technology purchase variables X_b^{bkW}, X_b^{bkWh}, X_t^{σ}, $X_{tks}^{s\sigma}$, and $Z_{tks}^{s\sigma}$ from $\mathcal{R}$. The hourly operational variable Y_h^{ω} from ($\mathcal{P}$) is mapped to X_{th}^{tp}, Z_{th}^{to}, X_{tuh}^{ptg}, X_{uh}^{stg}, X_{uh}^{g}, X_{bh}^{dfs}, X_{bth}^{pts}, X_h^{gts}, X_{th}^{f}, X_{th}^{tpb}, X_{th}^{tp}, X_{th}^{ptw}, and X_{th}^{fb} from ($\mathcal{R}$). Long-term operational decisions W^{ω} from ($\mathcal{P}$) can be mapped to Z_{de}^{dt}, X_{mn}^{dn}, Z_{mn}^{dmt}, Z_{mu}^{ut}, Z_v^{nmil}, X_{de}^{de}, X^{mc}, X^{plb}, Z_t^{pi}, and X_t^{pi} from ($\mathcal{R}$). The storage state-of-charge variable B_h^{ω} from ($\mathcal{P}$) can be mapped to $X_{b,0}^{\text{se}}$ and X_{bh}^{se} from ($\mathcal{R}$).

Constraint (4b) from ($\mathcal{P}$) corresponds to ($\mathcal{R}$) constraint set (A.7) as well as constraints (A.3a)–(A.3c) to define the feasible sizing of generating and storage technologies, respectively. Constraint (4c) from ($\mathcal{P}$) corresponds to ($\mathcal{R}$) constraint sets (A.1), (A.2), (A.4), (A.5), and (A.6) as well as constraints (A.3d)–(A.3g), (A.3l)–(A.3o), and (A.8a)–(A.8f). Constraint (4d) from ($\mathcal{P}$) corresponds to ($\mathcal{R}$) constraint sets (A.9), (A.10), (A.11), and (A.12) as well as constraint (A.13). Constraint (4e) was introduced in ($\mathcal{P}$) and corresponds to constraint (A.8g) in ($\mathcal{R}$). To maintain the established nomenclature from ($\mathcal{R}$), our original variable for unmet load, V_h^{ω} was updated to X_h^{uml}. Constraints (4f)–(4h) from ($\mathcal{P}$) correspond to ($\mathcal{R}$) constraints (A.3h)–(A.3k). The variables in ($\mathcal{P}$) are also subject to non-negativity and integrality constraints. In the interest of space, the non-negativity and integrality constraints presented in ($\mathcal{R}$) are grouped by variables with the same indices. As a result, some constraints from ($\mathcal{R}$) such as constraint (A.14a) correspond directly to constraint (4d) in ($\mathcal{P}$) while other constraints from ($\mathcal{R}$) such as constraint (A.14b) establish the non-negativity of variables X_t^{σ} and X_t^{pi} which correspond to constraints (4b) and (4c) from ($\mathcal{P}$), respectively. All variables, continuous and binary, are accounted for in the constraint sets (A.14) and (A.15). The variables within each individual non-negativity and integrality constraint can be mapped back to each variable and associated constraint in ($\mathcal{P}$).

References

[1] Billion-dollar weather and climate disasters: Overview | National Centers for Environmental Information (NCEI). 2020, https://www.ncdc.noaa.gov/billions/. [Accessed 01 May 2020].

[2] Do Vivian, McBrien Heather, Flores Nina M, Northrop Alexander J, Schlegelmilch Jeffrey, Kiang Mathew V, Casey Joan A. Spatiotemporal distribution of power outages with climate events and social vulnerability in the USA. Nature Commun 2023;14(1):2470, Number: 1 Publisher: Nature Publishing Group.

[3] Callahan Christopher W, Mankin Justin S. Globally unequal effect of extreme heat on economic growth. Sci Adv 2022;8(43):eadd3726.

[4] Villa Daniel L. Institutional heat wave analysis by building energy modeling fleet and meter data. Energy Build 2021;237:110774.

[5] Arrieta Felipe R Ponce, Lora Electo E Silva. Influence of ambient temperature on combined-cycle power-plant performance. Appl Energy 2005;80(3):261–72.

[6] Davenport Coral. Heat is costing the U.S. economy billions in lost productivity. 2023, https://www.nytimes.com/2023/07/31/climate/heat-labor-productivity-climate.html. [Accessed 2023-09-03].

[7] Stone Jr Brian, Mallen Evan, Rajput Mayuri, Broadbent Ashley, Krayenhoff E Scott, Augenbroe Godfried, Georgescu Matei. Climate change and infrastructure risk: Indoor heat exposure during a concurrent heat wave and blackout event in Phoenix, Arizona. Urban Clim 2021;36:100787.

[8] OAR US EPA. Climate change indicators: Heat waves. 2021, https://www.epa.gov/climate-indicators/climate-change-indicators-heat-waves. [Accessed 03 September 2023].

[9] Ringkjøb Hans-Kristian, Haugan Peter M, Solbrekke Ida Marie. A review of modelling tools for energy and electricity systems with large shares of variable renewables. Renew Sustain Energy Rev 2018;96:440–59.

[10] Akorede Mudathir Funsho, Hizam Hashim, Pouresmaeil Edris. Distributed energy resources and benefits to the environment. Renew Sustain Energy Rev 2010;14(2):724–34.

[11] Jiayi Huang, Chuanwen Jiang, Rong Xu. A review on distributed energy resources and MicroGrid. Renew Sustain Energy Rev 2008;12(9):2472–83.

[12] Confrey John, Etemadi Amir H, Stuban Steven MF, Eveleigh Timothy J. Energy storage systems architecture optimization for grid resilience with high penetration of distributed photovoltaic generation. IEEE Syst J 2019;14(1):1135–46.

[13] Scioletti Michael S, Newman Alexandra M, Goodman Johanna K, Zolan Alexander J, Leyffer Sven. Optimal design and dispatch of a system of diesel generators, photovoltaics and batteries for remote locations. Optim Eng 2017;18(3):755–92.

[14] Hirwa Jusse, Ogunmodede Oluwaseun, Zolan Alexander, Newman Alexandra M. Optimizing design and dispatch of a renewable energy system with combined heat and power. Optim Eng 2022;23(3):1–31.

[15] Perera ATD, Zhao Bingyu, Wang Zhe, Soga Kenichi, Hong Tianzhen. Optimal design of microgrids to improve wildfire resilience for vulnerable communities at the wildland-urban interface. Appl Energy 2023;335:120744.

[16] Totschnig Gerhard, Hirner Ricki, Müller Andreas, Kranzl Lukas, Hummel Marcus, Nachtnebel H-P, Stanzel Philipp, Schicker Irene, Formayer Herbert. Climate change impact and resilience in the electricity sector: The example of Austria and Germany. Energy Policy 2017;103:238–48.

[17] Takalani Rofhiwa, Bekker Bernard. Load and load growth models for rural microgrids, and how to future-proof designs. In: 2020 international SAUPEC/robMech/PRASA conference. 2020, p. 1–6.

[18] Mishra Sakshi, Pohl Josiah, Laws Nick, Cutler Dylan, Kwasnik Ted, Becker William, Zolan Alex, Anderson Kate, Olis Dan, Elgqvist Emma. Computational framework for behind-the-meter DER techno-economic modeling and optimization: REopt Lite. Energy Syst 2022;13(2):509–37.

[19] Mak Wai-Kei, Morton David P, Wood R Kevin. Monte Carlo bounding techniques for determining solution quality in stochastic programs. Oper Res Lett 1999;24(1):47–56.

[20] Wang Yi, Rousis Anastasios Oulis, Strbac Goran. On microgrids and resilience: A comprehensive review on modeling and operational strategies. Renew Sustain Energy Rev 2020;134:110313.

[21] Anderson Katherine H, DiOrio Nicholas A, Cutler Dylan S, Butt Robert S. Increasing resiliency through renewable energy microgrids. Int J Energy Sect Manage 2017;2(2).

[22] Sepúlveda-Mora Sergio B, Hegedus Steven. Resilience analysis of renewable microgrids for commercial buildings with different usage patterns and weather conditions. Renew Energy 2022;192:731–44.

[23] Eddy John, Miner Nadine E, Stamp Jason. Sandia's Microgrid Design Toolkit. Electr J 2017;30(4):62–7.

[24] Deforest Nicholas, Cardoso Goncalo, Brouhard Thomas. Distributed Energy Resources Customer Adoption Model (DER-CAM) v5.9. 2018, https://www.osti.gov/biblio/1477858. [Accessed 28 June 2023].

[25] Mashayekh Salman, Stadler Michael, Cardoso Gonçalo, Heleno Miguel. A mixed integer linear programming approach for optimal DER portfolio, sizing, and placement in multi-energy microgrids. Appl Energy 2017;187:154–68.

[26] HOMER - Hybrid renewable and distributed generation system design software. 2023, https://www.homerenergy.com/index.html. [Accessed 07 August 2023].

[27] Lambert Tom, Gilman Paul, Lilienthal Peter. Micropower system modeling with HOMER. In: Integration of alternative sources of energy. John Wiley & Sons, Ltd; 2005, p. 379–418.

[28] Robert Fabien Chidanand, Gopalan Sundararaman. From solar microgrid simulation to field deployment: Accuracy and uncertainties. In: 2018 7th international conference on renewable energy research and applications (ICRERA). 2018, p. 1109–14.

[29] Panteli M, Mancarella P. Modeling and evaluating the resilience of critical electrical power infrastructure to extreme weather events. IEEE Syst J 2017;11(3):1733–42.

[30] Younesi Abdollah, Shayeghi Hossein, Safari Amin, Siano Pierluigi. Assessing the resilience of multi microgrid based widespread power systems against natural disasters using Monte Carlo Simulation. Energy 2020;207:118220.

[31] Ascione Fabrizio, Bianco Nicola, De Masi Rosa Francesca, Mauro Gerardo Maria, Vanoli Giuseppe Peter. Resilience of robust cost-optimal energy retrofit of buildings to global warming: A multi-stage, multi-objective approach. Energy Build 2017;153:150–67.

[32] Wang Luhao, Li Qiqiang, Ding Ran, Sun Mingshun, Wang Guirong. Integrated scheduling of energy supply and demand in microgrids under uncertainty: A robust multi-objective optimization approach. Energy 2017;130:1–14.

[33] Konneh Keifa Vamba, Adewuyi Oludamilare Bode, Lotfy Mohammed Elsayed, Sun Yanxia, Senjyu Tomonobu. Application strategies of model predictive control for the design and operations of renewable energy-based microgrid: a survey. Electronics 2022;11(4):554.

[34] Hans Christian A, Sopasakis Pantelis, Raisch Jörg, Reincke-Collon Carsten, Patrinos Panagiotis. Risk-averse model predictive operation control of islanded microgrids. IEEE Trans Control Syst Technol 2019;28(6):2136–51.

[35] Xiang Yue, Liu Junyong, Liu Yilu. Robust energy management of microgrid with uncertain renewable generation and load. IEEE Trans Smart Grid 2015;7(2):1034–43.

[36] Wang Shasha, Gangammanavar Harsha, Ekşioğlu Sandra D, Mason Scott J. Stochastic optimization for energy management in power systems with multiple microgrids. IEEE Trans Smart Grid 2017;10(1):1068–79.

[37] Han Dongho, Lee Jay H. Two-stage stochastic programming formulation for optimal design and operation of multi-microgrid system using data-based modeling of renewable energy sources. Appl Energy 2021;291:116830.

[38] Arguez Anthony, Durre Imke, Applequist Scott, Vose Russell S, Squires Michael F, Yin Xungang, Heim Richard R, Owen Timothy W. NOAA's 1981–2010 US climate normals: An overview. Bull Am Meteorol Soc 2012;93(11):1687–97.

[39] Climate data online (CDO) | National Climatic Data Center (NCDC). 2023, https://www.ncei.noaa.gov/cdo-web/. [Accessed 12 April 2023].

[40] Hulme Mike, Mahony Martin. Climate change: What do we know about the IPCC? Prog Phys Geogr 2010;34(5):705–18.

[41] Riahi Keywan, van Vuuren Detlef P, Kriegler Elmar, Edmonds Jae, O'Neill Brian C, Fujimori Shinichiro, Bauer Nico, Calvin Katherine, Dellink Rob, Fricko Oliver, Lutz Wolfgang, Popp Alexander, Cuaresma Jesus Crespo, Kc Samir, Leimbach Marian, Jiang Leiwen, Kram Tom, Rao Shilpa, Emmerling Johannes, Ebi Kristie, Hasegawa Tomoko, Havlik Petr, Humpenöder Florian, Da Silva Lara Aleluia, Smith Steve, Stehfest Elke, Bosetti Valentina, Eom Jiyong, Gernaat David, Masui Toshihiko, Rogelj Joeri, Strefler Jessica, Drouet Laurent, Krey Volker, Luderer Gunnar, Harmsen Mathijs, Takahashi Kiyoshi, Baumstark Lavinia, Doelman Jonathan C, Kainuma Mikiko, Klimont Zbigniew, Marangoni Giacomo, Lotze-Campen Hermann, Obersteiner Michael, Tabeau Andrzej, Tavoni Massimo. The Shared Socioeconomic Pathways and their energy, land use, and greenhouse gas emissions implications: An overview. Global Environ Change 2017;42:153–68.

[42] Masson-Delmotte Valérie, Zhai Panmao, Pirani Anna, Connors Sarah L, Péan Clotilde, Berger Sophie, Caud Nada, Chen Y, Goldfarb L, Gomis MI, et al. Climate change 2021: The physical science basis. In: Contribution of working group I to the sixth assessment report of the intergovernmental panel on climate change. Vol. 2, 2021.

[43] Bauer Nico, Calvin Katherine, Emmerling Johannes, Fricko Oliver, Fujimori Shinichiro, Hilaire Jérôme, Eom Jiyong, Krey Volker, Kriegler Elmar, Mouratiadou Ioanna, et al. Shared socio-economic pathways of the energy sector–quantifying the narratives. Global Environ Change 2017;42:316–30.

[44] Eyring Veronika, Bony Sandrine, Meehl Gerald A, Senior Catherine A, Stevens Bjorn, Stouffer Ronald J, Taylor Karl E. Overview of the coupled model intercomparison project phase 6 (CMIP6) experimental design and organization. Geosci Model Dev 2016;9(5):1937–58.

[45] Villa Daniel L, Schostek Tyler, Govertsen Krissy, Macmillan Madeline. A stochastic model of future extreme temperature events for infrastructure analysis. Environ Model Softw 2023;105663.

[46] Chen Jie, Brissette François P. Comparison of five stochastic weather generators in simulating daily precipitation and temperature for the Loess Plateau of China. Int J Climatol 2014;34(10):3089–105, _eprint: https://onlinelibrary.wiley.com/doi/pdf/10.1002/joc.3896.

[47] Zhang Mingxi, Yang Xihua, Cleverly Jamie, Huete Alfredo, Zhang Hong, Yu Qiang. Heat wave tracker: A multi-method, multi-source heat wave measurement toolkit based on Google Earth Engine. Environ Model Softw 2022;147:105255.

[48] Li Xin, Ren Guoyu, Wang Suyan, You Qinglong, Sun Yinchuan, Ma Yang, Wang Dai, Zhang Wen. Change in the heatwave statistical characteristics over China during the climate warming slowdown. Atmos Res 2021;247:105152.

[49] EnergyPlus weather data. 2023, https://energyplus.net/weather. [Accessed 12 April 2023].

[50] Villa Daniel L, Carvallo Juan Pablo, Bianchi Carlo, Lee Sang Hoon. Multi-scenario extreme weather simulator application to heat waves. In: Proceeding of the building performance analysis conference and simBuild co-organized by ASHRAE and IBPSA-USA. 2022, p. 49–58.

[51] Villa Daniel. Multi-scenario extreme weather simulator GitHub repository. 2023, https://github.com/sandialabs/MEWS. [Accessed 31 July 2023].

[52] Villa Daniel L, Lee Sang Hoon, Bianchi Carlo, Carvallo Juan Pablo, Azaroff Illya, Mammoli Andrea, Schostek Tyler. Multi-scenario Extreme Weather Simulator application to heat waves: Ko'olauloa community resilience hub. Science and Technology for the Built Environment 2023;0(0):1–19.

[53] Chandramowli Shankar N, Felder Frank A. Impact of climate change on electricity systems and markets – A review of models and forecasts. Sustain Energy Technol Assess 2014;5:62–74.

[54] Azad Hanieh Borhan, Mekhilef Saad, Ganapathy Vellapa Gounder. Long-term wind speed forecasting and general pattern recognition using neural networks. IEEE Trans Sustain Energy 2014;5(2):546–53, Conference Name: IEEE Transactions on Sustainable Energy.

[55] Nowotarski Jakub, Liu Bidong, Weron Rafał, Hong Tao. Improving short term load forecast accuracy via combining sister forecasts. Energy 2016;98:40–9.

[56] Hyndman Rob J, Ahmed Roman A, Athanasopoulos George, Shang Han Lin. Optimal combination forecasts for hierarchical time series. Comput Statist Data Anal 2011;55(9):2579–89.

[57] Möhrlen Corinna, Bessa Ricardo J, Fleischhut Nadine. A decision-making experiment under wind power forecast uncertainty. Meteorol Appl 2022;29(3):e2077, _eprint: https://onlinelibrary.wiley.com/doi/pdf/10.1002/met.2077.

[58] Craig Michael T, Cohen Stuart, Macknick Jordan, Draxl Caroline, Guerra Omar J, Sengupta Manajit, Haupt Sue Ellen, Hodge Bri-Mathias, Brancucci Carlo. A review of the potential impacts of climate change on bulk power system planning and operations in the United States. Renew Sustain Energy Rev 2018;98:255–67.

[59] Craig Michael T, Wohland Jan, Stoop Laurens P, Kies Alexander, Pickering Bryn, Bloomfield Hannah C, Browell Jethro, De Felice Matteo, Dent Chris J, Deroubaix Adrien, Frischmuth Felix, Gonzalez Paula LM, Grochowicz Aleksander, Gruber Katharina, Härtel Philipp, Kittel Martin, Kotzur Leander, Labuhn Inga, Lundquist Julie K, Pflugradt Noah, van der Wiel Karin, Zeyringer Marianne, Brayshaw David J. Overcoming the disconnect between energy system and climate modeling. Joule 2022;6(7):1405–17.

[60] Herzmann Daryl. Iowa environmental mesonet :: ASOS/AWOS/METAR data. 2023, https://mesonet.agron.iastate.edu/request/download.phtml?network=AK_ASOS. [Accessed 24 May 2023].

[61] Sengupta Manajit, Xie Yu, Lopez Anthony, Habte Aron, Maclaurin Galen, Shelby James. The National Solar Radiation Database (NSRDB). Renew Sustain Energy Rev 2018;89:51–60.

[62] Kumar Abhishek, Singh Arvind R, Deng Yan, He Xiangning, Kumar Praveen, Bansal Ramesh C. A novel methodological framework for the design of sustainable rural microgrid for developing nations. IEEE Access 2018;6:24925–51.

[63] Bhattacharyya Subhes C, Palit Debajit. Mini-grid based off-grid electrification to enhance electricity access in developing countries: What policies may be required? Energy Policy 2016;94:166–78.

[64] Zolan Alexander J, Scioletti Michael S, Morton David P, Newman Alexandra M. Decomposing loosely coupled mixed-integer programs for optimal microgrid design. INFORMS J Comput 2021;33(4):1300–19.

[65] Teter Michael D, Newman Alexandra M, Weiss Martin. Consistent notation for presenting complex optimization models in technical writing. Surv Oper Res Manag Sci 2016;21(1):1–17.

[66] Hirwa Jusse, Zolan Alexander, Becker William, Flamand Tülay, Newman Alexandra. Optimizing design and dispatch of a resilient renewable energy microgrid for a South African hospital. Appl Energy 2023;348:121438.

[67] Rockafellar R Tyrrell, Wets Roger J-B. Scenarios and policy aggregation in optimization under uncertainty. Math Oper Res 1991;16(1):119–47.

[68] Gade Dinakar, Hackebeil Gabriel, Ryan Sarah M, Watson Jean-Paul, Wets Roger J-B, Woodruff David L. Obtaining lower bounds from the progressive hedging algorithm for stochastic mixed-integer programs. Math Program 2016;157:47–67.

[69] Wood Graham R. The bisection method in higher dimensions. Math Program 1992;55:319–37.

[70] Anderson Kate, Laws Nicholas D, Marr Spencer, Lisell Lars, Jimenez Tony, Case Tria, Li Xiangkun, Lohmann Dag, Cutler Dylan. Quantifying and monetizing renewable energy resiliency. Sustainability 2018;10(4).

[71] Anderson Kate, Olis Dan, Becker Bill, Parkhill Linda, Laws Nick, Li Xiangkun, Mishra Sakshi, Kwasnik Ted, Jeffery Andrew, Elgqvist Emma, Krah Kathleen, Cutler Dylan, Zolan Alex, Muerdter Nick, Eger Rob, Walker Andy, Hampel Chris, Tomberlin Gregg. REopt Lite user manual. Technical report NREL/TP-7A40-79235, National Renewable Energy Laboratory, Golden, CO (United States); 2021.

[72] Macmillan Madeline, Murphy Caitlin A, Bazilian Morgan D. Exploring acute weather resilience: Meeting resilience and renewable goals. Renew Sustain Energy Rev 2022;168.

[73] Narayan Apurva, Ponnambalam Kumaraswamy. Risk-averse stochastic programming approach for microgrid planning under uncertainty. Renew Energy 2017;101:399–408.

[74] Department of energy commercial reference buildings. 2020, https://www.energy.gov/eere/buildings/commercial-reference-buildings. [Accessed 28 April 2020].

[75] Husted Mark A, Suthar Bharatkumar, Goodall Gavin H, Newman Alexandra M, Kohl Paul A. Coordinating microgrid procurement decisions with a dispatch strategy featuring a concentration gradient. Appl Energy 2018;219:394–407.

[76] Goodall Gavin, Scioletti Michael, Zolan Alex, Suthar Bharatkumar, Newman Alexandra, Kohl Paul. Optimal design and dispatch of a hybrid microgrid system capturing battery fade. Optim Eng 2019;20:179–213.

[77] Dyreson Ana, Devineni Naresh, Turner Sean WD, De Silva M Thushara, Miara Ariel, Voisin Nathalie, Cohen Stuart, Macknick Jordan. The role of regional connections in planning for future power system operations under climate extremes. Earth's Future 2022;10(6):e2021EF002554.

[78] Polasky Andrew D, Evans Jenni L, Fuentes Jose D, Hamilton Holly L. Statistical climate model downscaling for impact projections in the midwest United States. Int J Climatol 2022;42(5):3038–55.

[79] Brodt-Giles Debbie, Buster Grant, Mooney Meghan, Day Megan, Rojas David. 2023 JISEA annual meeting: Addressing real life data challenges and novel solutions for applied science projects. Technical report, National Renewable Energy Laboratory (NREL), Golden, CO (United States); 2023.

[80] Ogunmodede Oluwaseun, Anderson Kate, Cutler Dylan, Newman Alexandra. Optimizing design and dispatch of a renewable energy system. Appl Energy 2021;287:116527.